JGR Oceans

RESEARCH ARTICLE
10.1029/2023JC020558

A Multi-Data Set Analysis of the Freshwater Transport by the Atlantic Meridional Overturning Circulation at Nominally 34.5°S

Cristina Arumí-Planas[1], Shenfu Dong[2], Renellys Perez[2], Matthew J. Harrison[3], Riccardo Farneti[4], and Alonso Hernández-Guerra[1]

[1]Unidad océano y clima, Instituto de Oceanografía y Cambio Global, IOCAG, Universidad de Las Palmas de Gran Canaria, ULPGC, Unidad Asociada ULPGC-CSIC, Las Palmas de Gran Canaria, Spain, [2]Atlantic Oceanographic and Meteorological Laboratory, National Oceanic and Atmospheric Administration, Miami, FL, USA, [3]Geophysical Fluid Dynamical Laboratory, National Oceanic and Atmospheric Administration, Princeton University, Princeton, NJ, USA, [4]The Abdus Salam International Centre for Theoretical Physics (ICTP), Trieste, Italy

Abstract The freshwater transport (M_{ov}) by the Atlantic Meridional Overturning Circulation (AMOC) across 34.5°S is computed using observations from 49 eXpendable BathyThermograph (XBT) transects between 2002 and 2019. The M_{ov} at 34.5°S serves as a possible indicator of the AMOC stability, with a negative (southward) freshwater transport indicating a possible bistable AMOC regime and positive (northward) transport indicating a monostable regime. A negative M_{ov} mean of -0.15 ± 0.09 Sv is estimated from the repeated XBT transects, suggesting a bistable AMOC regime. Results are complemented with two data sets derived from Argo float observations, numerical ocean models, and coupled climate models. More than half of the coupled models examined, 20 out of 32, present positive M_{ov} mean values. To investigate the causes of the differing signs of the M_{ov} across the models, we examine the salinity vertical structure in models with positive and negative M_{ov}, indicating fresher upper and saltier deep waters in models with positive M_{ov}. The South Atlantic meridional fluxes show linear relationships, with a negative slope (positively correlated in magnitude) between M_{ov}/MOC and M_{ov}/MHT, and a positive slope (positively correlated) between MHT/MOC. Seasonally, the South Atlantic meridional fluxes from most of the data sets considered here, show a more negative M_{ov} and a more positive MOC and MHT in austral fall and winter from April to August across 34.5°S.

Plain Language Summary It is well known that the meridional (north-south) overturning circulation, a large system of ocean currents driven by winds, buoyancy (density) differences, mixing, and eddies, has a significant impact on the world's climate system. Based on observations and numerical model data, this study presents a multi-data set analysis of the freshwater transported by this circulation system across the nominal latitude of 34.5°S in the South Atlantic. The observed southward meridional freshwater transport (out of the South Atlantic) derived from all the observational data sets considered indicates a bistable regime of the meridional overturning circulation. Some coupled models that suggest a mono-stable (one stable state) regime have fresher upper and saltier deep waters than the models that indicate a bistable regime (two stable states). We confirm that there is a linear relationship between mass transport by the meridional overturning circulation with the meridional freshwater and heat transports. Finally, we determine the seasonal variability of these meridional fluxes, with a more negative meridional freshwater transport, as well as a more positive overturning circulation volume and heat transports from April to August in the South Atlantic Ocean across 34.5°S.

Key Points:

- Observational-based estimates of negative freshwater transports by the AMOC (M_{ov}) at 34.5°S, suggest a bistable AMOC regime
- Many coupled models demonstrate positive M_{ov} values, attributed to biased salinity vertical profile patterns
- The M_{ov} is positively correlated in magnitude with mass and heat transport by the meridional overturning circulation

Correspondence to:
C. Arumí-Planas,
cristina.arumi@ulpgc.es

Citation:
Arumí-Planas, C., Dong, S., Perez, R., Harrison, M. J., Farneti, R., & Hernández-Guerra, A. (2024). A multi-data set analysis of the freshwater transport by the Atlantic meridional overturning circulation at nominally 34.5°S. *Journal of Geophysical Research: Oceans*, *129*, e2023JC020558. https://doi.org/10.1029/2023JC020558

Received 23 OCT 2023
Accepted 3 JUN 2024

Author Contributions:

Conceptualization: Cristina Arumí-Planas
Data curation: Cristina Arumí-Planas, Shenfu Dong, Renellys Perez, Matthew J. Harrison, Riccardo Farneti
Formal analysis: Cristina Arumí-Planas
Funding acquisition: Shenfu Dong, Renellys Perez, Matthew J. Harrison, Alonso Hernández-Guerra
Investigation: Cristina Arumí-Planas
Methodology: Cristina Arumí-Planas, Shenfu Dong, Renellys Perez
Project administration: Shenfu Dong, Renellys Perez, Matthew J. Harrison, Alonso Hernández-Guerra
Resources: Cristina Arumí-Planas, Shenfu Dong, Renellys Perez
Software: Cristina Arumí-Planas

1. Introduction

One of the key questions in climate studies is how the Atlantic Meridional Overturning Circulation (AMOC) will respond to the effects of global warming and subsequent alterations in the hydrological cycle (de Vries & Weber, 2005; Keller et al., 2000). The oceans play an essential role as a redistribution agent and global reservoir for several important constituents, such as heat, freshwater, and carbon, of the Earth's climate system. The AMOC is a crucial element of the Atlantic Ocean climate system, as it carries heat northward at all latitudes, thereby warming surface air temperatures in Western Europe (Ganachaud & Wunsch, 2000; Mecking et al., 2017; Talley, 2003). As a result, a weakening or even collapse of the AMOC could lead to a strong cooling of surface air temperatures in regions surrounding the North Atlantic (Jackson et al., 2015; Manabe & Stouffer, 1988; Vellinga & Wood, 2002), and a convergence of warm water in the tropical and subtropical North Atlantic, which could lead

Supervision: Shenfu Dong, Renellys Perez, Alonso Hernández-Guerra
Validation: Cristina Arumí-Planas, Shenfu Dong, Renellys Perez, Alonso Hernández-Guerra
Visualization: Cristina Arumí-Planas
Writing – original draft: Cristina Arumí-Planas
Writing – review & editing: Cristina Arumí-Planas

to weaker and less frequent Atlantic hurricanes (Yan et al., 2017). It is important to understand the interplay between AMOC-induced cooling and background global warming, as Liu et al. (2020) did in a numerical modeling study focused on the 21st century.

In the southernmost latitude of the Atlantic Ocean, nominally 34.5°S, the freshwater transport by the AMOC, referred to as M_{ov} hereafter, is used as a possible indicator of the AMOC bistability with significant global climate effects (Cimatoribus et al., 2012; de Vries & Weber, 2005; Huisman et al., 2010; Matos et al., 2020; Mecking et al., 2016, 2017; Rahmstorf, 1996; Skliris et al., 2020). The South Atlantic Ocean has historically been less studied than the North Atlantic, as a result, model estimates of the M_{ov} have been poorly constrained in this basin (Garzoli et al., 2013; Weijer et al., 2019). Nevertheless, the repeated high-density eXpendable BathyThermograph (XBT) lines (trans-basin AX18 line from South America to Cape Town; AX22 and AX25 lines across the Drake Passage and the Agulhas retroflection, respectively), together with the Argo program collecting a large number of temperature and salinity profiles (Roemmich & Owens, 2000), and the quasi-decadal occupation of trans-basin hydrographic lines (Arhan et al., 2003; Arumí-Planas et al., 2023; Bryden et al., 2011; Hernández-Guerra et al., 2019; Manta et al., 2021; McDonagh & King, 2005; Saunders & King, 1995) have increased data coverage in the South Atlantic region. Consequently, observed and simulated estimates of mean AMOC and Meridional Heat Transport (MHT) in the South Atlantic have become more consistent over the last decade (Baringer & Garzoli, 2007; Chidichimo et al., 2023; Dong et al., 2009, 2011; Kersalé et al., 2021; Pita et al., 2024; Sitz et al., 2015; Weijer et al., 2020), with fairly good agreement in terms of AMOC and MHT variability between models and some observations in more recent studies (Baker et al., 2023; Biastoch et al., 2021; Dong et al., 2021). However, previous estimations of freshwater transport from observations are limited in the South Atlantic, and models and observations have shown disagreement about the freshwater transport direction in this region (e.g., Bryden et al., 2011; Caínzos et al., 2022; de Vries & Weber, 2005; Dijkstra, 2007; Drijfhout et al., 2011; Garzoli et al., 2013; Huisman et al., 2010; Liu et al., 2014, 2017; Weijer & Dijkstra, 2003).

The main goal of this study is to present a multi-data set analysis of the M_{ov} at nominally 34.5°S in the South Atlantic Ocean, using an updated AX18-XBT data set from April 2002 to October 2019 (following Garzoli et al. (2013) which only analyzed transects through 2011). Furthermore, we have examined the consistency between observed and simulated multidecadal variability of the South Atlantic meridional fluxes using two data sets derived from Argo floats measurements, Ocean General Circulation Models (OGCMs), and Coupled General Circulation Models (CGCMs), and we have diagnosed the causes of the differences in the sign of M_{ov}. Finally, we have analyzed the seasonal variability of South Atlantic meridional fluxes and examined how the fluxes covary on longer timescales.

2. Data and Methods

2.1. Observational and Numerical Model Data

In this study, our focus is on the variability of the M_{ov} nominally across 34.5°S in the South Atlantic and how it covaries with meridional mass (or volume which is strongly linked to mass transport) and heat transports by the overturning circulation. As our primary data set, we have used 49 realizations of the AX18 repeat high-density XBT line from April 2002 to October 2019. The 49 transects of the AX18-XBT line used in this study are presented in Figure 1. These transects were conducted using Evergreen container ships that crossed the South Atlantic from South America to South Africa. AX18-XBT measures water temperature profiles from the sea surface to a nominal depth of 850 m. Salinity profiles were generated using a historical T-S relationship (Goes et al., 2018). To extend the T & S profiles down to the seafloor, we utilized the 1/4° horizontal resolution NCEI World Ocean Atlas 2018 (WOA18) T-S climatology. Specifically, we used monthly averages of WOA18 data between 800–1,500 m and seasonal averages below 1,500 m (Garcia et al., 2019; Locarnini et al., 2018; Zweng et al., 2019). This data set comprises 57 vertical levels spanning from 0 to 1,500 m for the monthly averages, while it encompasses 112 vertical levels spanning from 0 to 5,500 m for seasonal averages. Then, each T-S profile is linearly interpolated from the surface to the seafloor with 140 predefined depths, using intervals of 5–10 m up to 750 m, 50 m intervals until 2,000 m, and finally, 100 m intervals reaching the seafloor. The T-S relationship method for estimating the mass transport from XBT data presents an uncertainty that might be similar to that estimated by Hernández-Guerra et al. (2002) for the region of the Canary Islands. The Ekman transport contribution is computed using NCEP annual mean winds and is included in the shallowest layer, employing the same methodology as outlined in both Baringer & Garzoli (2007) and Garzoli & Baringer (2007).

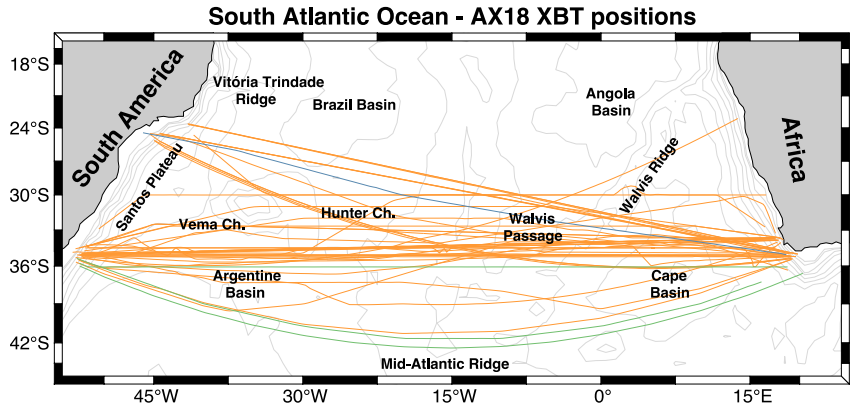

Figure 1. Locations of the high-density AX18-XBT lines conducted in the South Atlantic Ocean. The green color lines correspond to the individual AX18-XBT transects for which positive M_{ov} values were observed, whereas the blue line represents the transect exhibiting large negative M_{ov}.

The AX18-XBT data were complemented with data from Argo floats and different simulations of OGCMs and CGCMs across 34.5°S in the Atlantic Ocean, as described below.

The first data set used to compare with the AX18-XBT results in this study is monthly data from the Argo Altimetry product (Argo Alt. hereafter). The Argo Alt. consists of the daily sea level anomaly (SLA) observations processed and distributed by the Copernicus Marine Environment Monitoring Service (CMEMS) (Pujol et al., 2016), as well as temperature and salinity (T-S) profiles from the Global Temperature and Salinity Profile Program (GTSPP) (Sun et al., 2010) (Argo Alt. hereafter). The Argo Alt. data set has a 0.25° horizontal resolution and is available from January 1993 to August 2022, with 305 vertical levels from the surface to the bottom of the ocean (Dong et al., 2015, 2021).

The Roemmich-Gilson (RG) Argo Climatology, RG Argo hereafter, is the next data set used in this study. This data set provides monthly gridded hydrographic salinity-temperature profiles based on the Argo Buoy Observation Network (Roemmich & Gilson, 2009). The RG Argo has a 1° horizontal resolution and 58 vertical levels from 2.5 to 1,975 dbar. For this study, we used data in the South Atlantic Ocean across 34.5°S, covering the period from January 2004 to August 2022. The gridded-field RG Argo was estimated based on a weighted least-squares fitting method that utilized the nearest 100 Argo profiles within a given month. Potential density, steric height, and relative geostrophic velocity with the reference layer at 1,000 m depth were calculated using the salinity and temperature fields from 223 months of data. In addition, the velocities at the parking depth (1,000 m) from the YoMaHa data set were summed to the RG Argo derived relative geostrophic velocity profiles to provide an absolute velocity (Lebedev et al., 2007).

The Ocean general circulation model For the Earth Simulator (OFES) run by the Japan Agency for Marine-Earth Science and Technology (JAMSTEC) is the first OGCM examined in this study. This high-resolution eddy-resolving model has a horizontal resolution of 0.1° and 54 vertical levels from the surface to the ocean bottom. To simulate ocean circulation, the OFES model was spun up for 50 years using a monthly climatology derived from NCEP/NCAR reanalysis atmospheric fluxes (Masumoto et al., 2004), and then was forced with daily mean NCEP/NCAR reanalysis data from 1950 to 2017 (Sasaki et al., 2008). Model fields were provided by JAMSTEC at the full resolution (0.1°) for the region across 34.5°S in the Atlantic Ocean, covering the period from January 1980 to December 2017.

The second OGCM, the GLORYS12V1 model (Global Ocean Physics Reanalysis; GLORYS, hereafter) developed by the CMEMS, examined in this study is an eddy-resolving global ocean reanalysis model. GLORYS is based on the current real-time global forecasting CMEMS system. The model hydrodynamics are based on NEMO (Nucleus for European Modeling of the Ocean) and assimilates in situ observations from the CORA4 database and atmospheric forcing from ERA-Interim data. Additionally, it assimilates altimeter data (sea level anomaly), sea ice concentration, satellite sea surface temperature, and in situ temperature and salinity vertical profiles. This results in monthly gridded data sets with a horizontal resolution of 1/12° and 50 vertical levels from

the surface to the seafloor (Drévillon et al., 2018). GLORYS12V1 data from January 1993 to December 2019 are used in this study.

The Geophysical Fluid Dynamics Laboratory (GFDL) OM4 ocean/sea ice model (Adcroft et al., 2019) is the third OGCM used in this study. The ocean component of OM4 uses the Modular Ocean Model version 6, forced with the JRA55-do atmospheric reanalysis product (Tsujino et al., 2020; MOM6-JRA, hereafter), and monthly averages were stored for the entire simulation period. MOM6-JRA has a nominal horizontal spacing of 0.25°, with no mesoscale eddy parameterization and 50 vertical levels spanning from the surface to the ocean bottom. MOM6-JRA data from January 1988 to December 2017 are used in this study. MOM6-JRA dynamical core is based on hydrostatic primitive equations formulated in their generalized vertical coordinate form.

A second MOM6 simulation using MERRA-2 forcing is the fourth OGCM included in this study (Rienecker et al., 2011; MOM6-MERRA2, hereafter). MOM6-MERRA2 has a nominal 0.25° horizontal spacing and 35 vertical levels spanning from the ocean surface to the bottom. Differences between the MOM6 simulations can be primarily attributed to the atmospheric forcing used. MERRA2 reanalysis includes an adjustment of precipitation and evaporation over both the ocean and the earth's surface (Harrison et al., 2022). Additionally, the MERRA2 atmospheric forcing covers a more recent period as it extends up to December 2020.

Finally, monthly outputs from 32 historical CGCM simulations from the Coupled Model Intercomparison Project 6 (CMIP6) for the period 1850–2014 have been used in this study. CMIP6 models were obtained from the Earth System Grid Data Portal, but not all the CMIP6 models have the "r1i1p1f1" ensemble member available. Therefore, we have used different ensemble members when the first is not available, as indicated in Table 1. The corresponding institution for each model, experiment ID ("Historical"), member ID, horizontal resolution (usually 1°), and citation are also included in Table 1. A multi-model mean is computed using the 32 CMIP6 models for comparison with other data sets.

For all data sets considered in this study, we have examined statistics such as mean and trends over the full period of each data set, as well as over the years 2004–2014 which is the period of overlap among all the observations and models used.

To compare the vertical profiles from the CGCMs with observations, we have used salinity and temperature profiles from hydrographic data collected at nominally 34.5°S in the Atlantic Ocean which will be referred to as MSM60 in the figures.

2.2. M_{ov}, MOC, and MHT Calculations

The total freshwater and heat transports can be divided into components corresponding to different driving mechanisms of vertical and horizontal circulation in the ocean, allowing for the breakdown of these transports into barotropic (throughflow), baroclinic (overturning), and horizontal (gyre) components (Bryden & Imawaki, 2001; Caínzos et al., 2022; Kersalé et al., 2021). In this study, we have only focused on the overturning component of freshwater transport (M_{ov}). The oceanic freshwater transport is the part of mass transport that is not saline. Its divergence can be understood as the balance of precipitation, river runoff, ice processes, and evaporation. To calculate it, the salt flux (or the non-freshwater portion of the mass transport) is constrained across the section, remaining unaffected by the strength of the freshwater divergence, given that this occurs at zero salinity. In this study, we have computed the M_{ov} as the zonally averaged vertical circulation of the salt at a specific zonal section at 34.5°S in Sverdrup units (1 Sv = 10^9 kg/s), following McDonagh et al. (2015) and Caínzos et al. (2022):

$$M_{ov} = -\frac{1}{S_0}\int_{-B}^{0} \rho\, \overline{v^*}(z)\langle S'(z)\rangle dz$$

where S_o is the area-weighted section average of salinity, z represents depth, $-B$ is the depth of the ocean bottom, ρ is the seawater density, $\overline{v^*}(z)$ is the meridional baroclinic ocean velocity and overbar denotes zonal integral, and $\langle S'(z)\rangle$ denotes the area-weighted zonally averaged deviations from the salinity average, S_o. Following this equation, we have also computed the Ekman contribution to the M_{ov} for the AX18-XBT sections, resulting in a mean transport of -0.03 ± 0.05 Sv within the Ekman layer. Unfortunately, due to the difficulty of consistently identifying the time-varying depth of the interface between the AABW and NADW cells across all observations and models, we have only integrated M_{ov} down to $z = -B$.

Table 1
List of the 32 Coupled Global Climate Models (CGCMs) From the CMIP6 Project

Source ID	Institute ID	Experiment ID	Member ID	Resolution	Citation
TaiESM1	AS-RCEC	Historical	r1i1p1f1	1.13°	Lee and Liang (2020)
BCC-CSM2-MR	BCC	Historical	r1i1p1f1	1.00°	Wu et al. (2018)
BCC-ESM1	BCC	Historical	r1i1p1f1	1.00°	Zhang et al. (2018)
FGOALS-g3	CAS	Historical	r1i1p1f1	1.00°	Li (2019)
CanESM5	CCCma	Historical	r10i1p2f1	1.00°	Swart et al. (2019)
CMCC-CM2-SR5	CMCC	Historical	r1i1p1f1	1.00°	Lovato and Peano (2020)
CMCC-ESM2	CMCC	Historical	r1i1p1f1	1.00°	Lovato et al. (2021)
CNRM-CM6-1	CNRM-CERFACS	Historical	r2i1p1f2	1.00°	Voldoire (2018)
CNRM-ESM2-1	CNRM-CERFACS	Historical	r1i1p1f2	1.00°	Seferian (2018)
ACCESS-ESM1-5	CSIRO	Historical	r1i1p1f1	1.00°	Ziehn et al. (2019)
ACCESS-CM2	CSIRO-ARCCSS	Historical	r1i1p1f1	1.00°	Dix et al. (2019)
E3SM-1-0	E3SM Project	Historical	r1i1p1f1	1.00°	Bader et al. (2019a)
E3SM-1-1	E3SM Project	Historical	r1i1p1f1	1.00°	Bader et al. (2019b)
EC-Earth3	EC-Earth Consortium	Historical	r10i1p1f1	1.00°	EC-Earth (2019)
EC-Earth3-AerChem	EC-Earth Consortium	Historical	r1i1p1f1	1.00°	EC-Earth (2020)
IPSL-CM6A-LR	IPSL	Historical	r22i1p1f1	1.00°	Boucher et al. (2018)
MIROC-ES2L	MIROC	Historical	r2i1p1f2	1.00°	Hajima et al. (2019)
MIROC6	MIROC	Historical	r2i1p1f1	1.00°	Tatebe and Watanabe (2018)
HadGEM3-GC31-LL	MOHC	Historical	r1i1p1f3	1.00°	Ridley et al. (2019)
UKESM1-0-LL	MOHC	Historical	r1i1p1f2	1.00°	Tang et al. (2019)
MPI-ESM1-2-HR	MPI-M	Historical	r1i1p1f1	0.45°	Jungclaus et al. (2019)
GISS-E2-1-G	NASA-GISS	Historical	r1i1p1f1	1.25°	NASA/GISS (2018)
GISS-E2-1-G-CC	NASA-GISS	Historical	r1i1p1f1	1.25°	NASA/GISS (2019)
CESM2	NCAR	Historical	r10i1p1f1	1.13°	Danabasoglu (2019b)
CESM2-WACCM	NCAR	Historical	r1i1p1f1	1.13°	Danabasoglu (2019a)
NorESM2-LM	NCC	Historical	r1i1p1f1	1.00°	Seland et al. (2019)
NorESM2-MM	NCC	Historical	r1i1p1f1	1.00°	Bentsen et al. (2019)
GFDL-CM4	NOAA-GFDL	Historical	r1i1p1f1	0.25°	Guo et al. (2018)
NESM3	NUIST	Historical	r1i1p1f1	1.00°	Cao and Wang (2019)
SAM0-UNICON	SNU	Historical	r1i1p1f1	1.13°	Park and Shin (2019)
CIESM	THU	Historical	r1i1p1f1	1.13°	Huang (2019)
MCM-UA-1-0	UA	Historical	r1i1p1f1	1.88°	Stouffer (2019)

Note. For each model, the corresponding modeling center, experiment ID, member ID, horizontal resolution, and citation are indicated. Ten out of the 32 models did not have the "r1i1p1f1" ensemble member available.

The M_{ov} is a diagnostic for basin-wide salt-advection feedback in the southern border of the Atlantic Ocean and it is widely considered an indicator for monitoring the stability of the AMOC (Bryden et al., 2011; de Vries & Weber, 2005; Dijkstra, 2007; Drijfhout et al., 2011; Gent, 2018; Liu et al., 2017; Matos et al., 2020; Rahmstorf, 1996; Weber & Drijfhout, 2007; Weijer et al., 2019). At approximately 34.5°S, a positive value of the M_{ov} (freshwater convergence) indicates that the AMOC is importing freshwater into the Atlantic, while a negative M_{ov} value (freshwater divergence) indicates that the AMOC is exporting freshwater from the Atlantic Basin. If the AMOC shuts down or weakens dramatically, M_{ov} would weaken and be closer to zero. Then, a positive (negative) change in the M_{ov} would occasion an anomalous import of salt (freshwater) into the Atlantic Ocean and as a result, the AMOC will destabilize (establish) the AMOC off-state (Mecking et al., 2017). Therefore, a $M_{ov} > 0$ provides a monostable AMOC and, conversely, a $M_{ov} < 0$ provides a bistable AMOC (Bryden et al., 2011; Caínzos

et al., 2022; Garzoli et al., 2013; McDonagh & King, 2005; Mecking et al., 2017; Saunders & King, 1995; Stommel, 1961; Weijer et al., 1999). It is worth noting that the sign of the M_{ov} at 34.5°S is not the only indicator for considering the multiple equilibrium regimes of the AMOC. One critical issue is that in climate models, the idealized hypothesis from Rahmstorf's (1996) box model may not be valid for the CGCM, as the collapsed AMOC has a minor strength of 3–4 Sv and induces a nonzero M_{ov} across the Atlantic basin (Liu et al., 2013). According to Dijkstra (2007), Huisman et al. (2010), and Yin & Stouffer (2007), another valuable parameter for assessing AMOC stability is the divergence of the M_{ov} between two latitudes in the North Atlantic Subtropical Gyre (i.e., 35°S and 60°N). Additionally, Liu & Liu (2013, 2014), suggest examining the difference between the M_{ov} across 34.5°S and the overturning liquid freshwater transport from the Arctic to the North Atlantic Ocean as an improved divergence indicator of AMOC stability, although this is not always possible to estimate M_{ov} divergence from in situ observations. More recently, van Westen et al. (2024) demonstrated that the M_{ov} minima at 34°S in the Atlantic coincides with the AMOC tipping point. Altogether, it's important to note that the M_{ov} at 34.5°S consistently appears as an important term in all these studies.

The meridional mass transport by AMOC across 34.5°S for the Atlantic Ocean is computed by zonally and vertically integrating the mass transport from the ocean's surface to its bottom, measured in Sv (e.g., Frajka-Williams et al., 2019). The intensity of the overturning, MOC, is typically defined as the maximum value in the overturning stream function in the upper cell. Thus, the strength of the MOC can be expressed as:

$$\mathrm{MOC} = \int_{-M}^{0} \int_{x_{\mathrm{west}}}^{x_{\mathrm{east}}} \rho\, v\,(x,z)\, dx\, dz$$

which is integrated over depth (z) and across the section from west (x_{west}) to east (x_{east}), where ρ is the seawater density, v represents the absolute meridional velocities, and $-M$ is the depth of the maximum overturning stream function. A positive MOC indicates northward mass transport and a negative MOC suggests southward mass transport. Some estimates of the MOC from moored arrays compute the volume transport by the AMOC rather than mass transport (e.g., Chidichimo et al., 2023; Frajka-Williams et al., 2019), and these transports can be considered interchangeable.

The MHT is computed at a zonal section at latitude 34.5°S, in Petawatts (1 PW = 10^{15} W), by using the following expression:

$$\mathrm{MHT} = \int_{-B}^{0} \int_{x_{\mathrm{west}}}^{x_{\mathrm{east}}} \rho\, c_p\, \theta(x,z)\, v(x,z)\, dx\, dz$$

which is integrated over depth (z) and across the section from west (x_{west}) to east (x_{east}), where ρ is the seawater density, c_p is the heat capacity of the seawater, θ is the potential temperature, v is the absolute meridional velocities, and $-B$ is the depth of the ocean bottom. A positive value of MHT indicates northward heat transport, whereas a negative value suggests southward heat transport. The mean and standard deviation of M_{ov}, MOC, and MHT for Argo Alt., RG Argo, OFES, GLORYS, MOM6-JRA, MOM6-MERRA, and CMIP6-mean are computed without considering seasonal variability. Therefore, we have first computed the annual mean for each year and, subsequently, the mean and standard deviation.

3. Results

3.1. XBT Data Analysis

The 49 AX18-XBT realizations from 2002 to 2019 have a negative mean of M_{ov} at 34.5°S in the Atlantic Ocean of -0.15 ± 0.09 Sv (Table 2). Only three transects have positive M_{ov} values: September 2014, May 2016, and May 2017 (Figure 2a). Two of these transects, September 2014 and May 2017, followed a bowed southerly path between South America and South Africa (green lines in Figure 1), and as a result, sampled through different water masses and can be considered as outliers. The positive M_{ov} trends presented in Table 2, suggest a slightly decreasing negative M_{ov} during the full period of the AX18-XBT data at a rate of 0.0033 ± 0.0049 Sv/year, but the positive trend is not statistically different from zero. During the overlapping period among all data sets, from 2004 to 2014, AX18-XBT data similarly show a non-significant decrease (positive trend) in M_{ov}.

Table 2
Mean, Trends, and 95% Confidence Intervals (CI) for M_{ov} (Sv), MOC (Sv), and MHT (PW) Derived From AX18-XBT Transects Nominally Across 34.5°S in the South Atlantic for Two Periods: Full Record Length (2002–2019) and Overlapping Period Among All Data Sets Analyzed (2004–2014)

Meridional transports		2002–2019	2004–2014
M_{ov}	Mean (Sv)	−0.15 ± 0.09	−0.16 ± 0.09
	Trends and 95% CI (Sv/year)	0.0033 ± 0.0049	0.0053 ± 0.0091
MOC	Mean (Sv)	19.6 ± 2.9	19.3 ± 2.7
	Trends and 95% CI (Sv/year)	0.1713 ± 0.1589	0.1677 ± 0.2789
MHT	Mean (PW)	0.59 ± 0.16	0.59 ± 0.16
	Trends and 95% CI (PW/year)	0.0034 ± 0.0090	0.0015 ± 0.0168

Note. Trends are given in units of Sv/year for M_{ov} and MOC, and in PW/year for MHT.

In addition, we have estimated the mean MOC (Figure 2b) and MHT (Figure 2c) from the AX18-XBT time series, which are 19.6 ± 2.9 Sv and 0.59 ± 0.16 PW, respectively (Table 2), consistent with previous estimates of northward mass and heat transport across 34.5°S in the South Atlantic. Both MOC and MHT have been strengthening throughout the full data set at a rate of 0.1713 ± 0.1589 Sv/year and 0.0034 ± 0.0090 PW/year, respectively (the increasing trend is only significant with 95% confidence for MOC). During the overlapping period of 2004–2014, MOC and MHT also show positive trends but are not significantly different from zero.

3.2. Comparison With Two Argo-Derived Data Sets

We have similarly estimated the M_{ov} using two different Argo-derived products to complement the AX18-XBT observations (red and blue lines, respectively, in Figure 3a). In both Argo time series, M_{ov} is always negative. When averaged over the overlapping period (2004–2014), both Argo data sets have a negative M_{ov} mean, −0.18 ± 0.02 Sv from Argo Alt. and −0.14 ± 0.01 Sv from RG Argo, in good agreement with the AX18-AX18-XBT M_{ov} mean of −0.15 ± 0.09 Sv (Figure 3a and Table 3). During the overlapping period of 2004–2014 among all observational and model data sets, the positive M_{ov} trends in the Argo Alt. and RG Argo time series indicate a non-significant weakening of the M_{ov}, similar to the AX18-XBT trend. However, M_{ov} trends are only significant for the full period of both Argo Alt. and RG Argo data sets. Over the full record length of Argo Alt. (1993–2022) and RG Argo (2004–2022), both data sets have weak but significant negative (increasing) M_{ov} trends.

The time series of MOC from Argo Alt. has a mean MOC of 19.3 ± 0.8 Sv, which is similar to the results obtained from AX18-XBT data (19.3 ± 2.7 Sv), while the RG Argo presents a significantly weaker MOC with a mean of 13.4 ± 0.4 Sv (Figure 3b and Table 3). The time series of MHT from Argo Alt. and RG Argo with a mean of

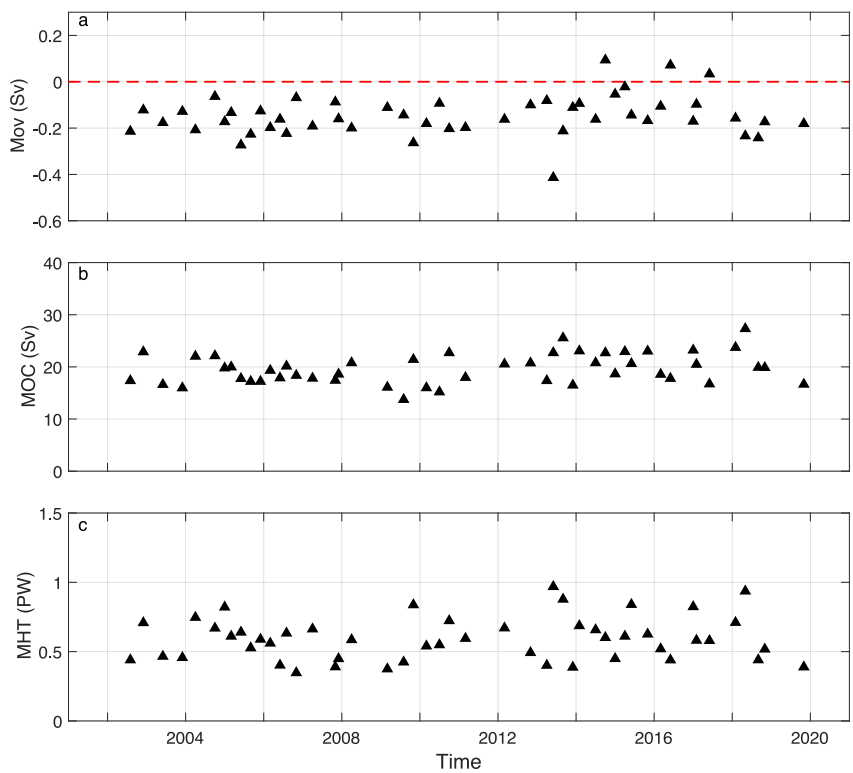

Figure 2. Time series of (a) M_{ov} (Sv), (b) MOC (Sv), and (c) MHT (PW) in the South Atlantic nominally across 34.5°S from 49 AX18-XBT section estimates (black triangles) for the period 2002–2019.

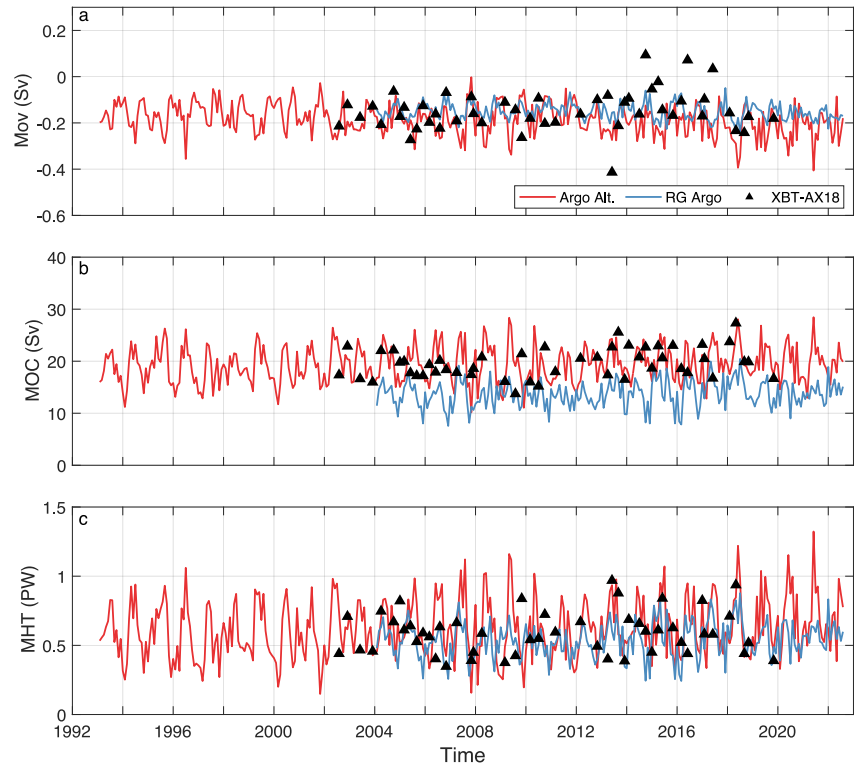

Figure 3. Time series of (a) M_{ov} (Sv), (b) MOC (Sv), and (c) MHT (PW) in the South Atlantic nominally across 34.5°S derived from observational data from AX18-XBT (black triangles), Argo Alt. (red solid line), and RG Argo (dark-blue solid line) estimates for the period 2002–2019, 1993–2022, and 2004–2022, respectively.

0.62 ± 0.04 PW and 0.52 ± 0.02 PW, respectively, agree with that obtained from AX18-XBT data (0.59 ± 0.16 PW) (Figure 3c and Table 3). The time series of the MOC and MHT (Figures 3b and 3c), as well as their trends, measured at 95% confidence intervals, from Argo Alt. and RG Argo data (Table 3), show that both meridional fluxes have been strengthening (0.0478–0.0655 Sv/year and 0.0034–0.0041 PW/year, respectively) throughout

Table 3
Mean Without Considering Seasonal Variability, Trends, and 95% Confidence Intervals (CI) of M_{ov} (Sv), MOC (Sv), and MHT (PW) From Observational Data From AX18-XBT, Argo Alt. and RG Argo Nominally Across 34.5°S in the South Atlantic for Two Periods: Full Record Length (AX18-XBT: 2002–2019, Argo Alt.: 1993–2022, and RG Argo: 2004–2022) and the Overlapping Period (2004–2014)

Meridional transports			AX18-XBT	Argo Alt.	RG Argo
M_{ov}	Mean (Sv)	Full record length	−0.15 ± 0.09	−0.19 ± 0.03	−0.15 ± 0.01
		2004–2014	−0.16 ± 0.09	−0.18 ± 0.02	−0.14 ± 0.01
	Trends and 95% CI (Sv/year)	Full record length	0.0033 ± 0.0049	−0.0020 ± 0.0008	−0.0011 ± 0.0009
		2004–2014	0.0053 ± 0.0091	0.0011 ± 0.0035	0.0011 ± 0.0018
MOC	Mean (Sv)	Full record length	19.6 ± 2.9	19.3 ± 0.9	13.8 ± 0.8
		2004–2014	19.3 ± 2.7	19.3 ± 0.8	13.4 ± 0.4
	Trends and 95% CI (Sv/year)	Full record length	0.1713 ± 0.1589	0.0478 ± 0.0421	0.0655 ± 0.0617
		2004–2014	0.1677 ± 0.2789	−0.0002 ± 0.1965	−0.0262 ± 0.1293
MHT	Mean (PW)	Full record length	0.59 ± 0.16	0.62 ± 0.05	0.54 ± 0.04
		2004–2014	0.59 ± 0.16	0.62 ± 0.04	0.52 ± 0.02
	Trends and 95% CI (PW/year)	Full record length	0.0034 ± 0.0090	0.0041 ± 0.0025	0.0034 ± 0.0031
		2004–2014	0.0015 ± 0.0168	−0.0012 ± 0.0113	−0.0026 ± 0.0063

Note. Trends are given in units of Sv/year for M_{ov} and MOC, and in PW/year for MHT.

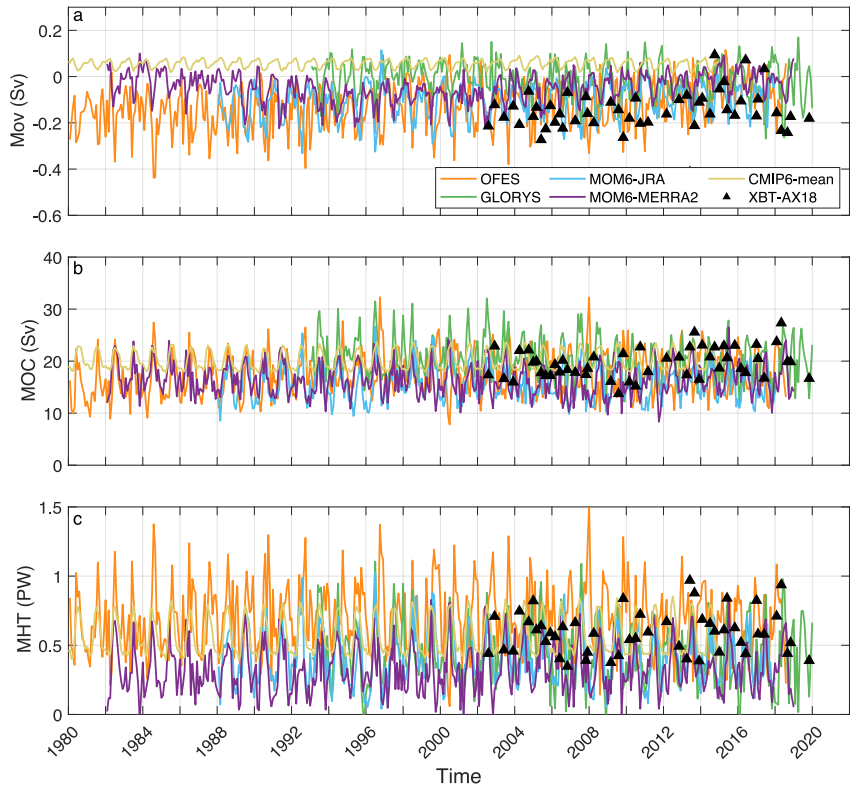

Figure 4. Time series of (a) M_{ov} (Sv), (b) MOC (Sv), and (c) MHT (PW) in the South Atlantic across 34.5°S from observational AX18-XBT derived data (black triangles) and numerical modeling data from OFES (orange solid line), GLORYS (green solid line), MOM6-JRA (light-blue solid line), MOM6-MERRA2 (purple solid line), and CMIP6-mean (yellow solid line) monthly data for the period 1980–2020.

the full record of each data set. During the overlapping period, both Argo products suggest a small weakening of the MOC and MHT, which have the opposite sign from the trends estimated from XBT-derived data (Table 3). However, the trends for MOC and MHT are only significant for the full period of both Argo Alt. and RG Argo data sets.

3.3. Comparison With OGCMs and CGCMs Data

Next, we have estimated the M_{ov} using different ocean and coupled numerical models: OFES, GLORYS, MOM6-JRA, MOM6-MERRA, and CMIP6 ensemble mean (hereafter CMIP6-mean), to further complement our AX18-XBT observations. The time series of M_{ov} from the OGCMs have predominantly negative values, with mean M_{ov} values of -0.11 ± 0.04 Sv for OFES and -0.09 ± 0.02 Sv for MOM6-JRA, which do not significantly differ from the AX18-XBT M_{ov} mean of -0.15 ± 0.09 Sv, except -0.03 ± 0.02 Sv for GLORYS and -0.03 ± 0.02 Sv for MOM6-MERRA2 which present lower negative M_{ov} mean (Figure 4a and Table 4). However, in contrast to negative M_{ov} values from observations and models mentioned above, the M_{ov} time series of the CMIP6-mean has a positive mean with a large standard deviation (0.06 ± 0.15 Sv; Figure 4a and Table 4). Consistent with the AX18-XBT data, the trends in the model time series, presented in Figure 4 and Table 4, all indicate a positive (weakening) M_{ov} trend during the overlapping period except for the CMIP6-mean. However, only the MOM-MERRA2 and CMIP6-mean have a significant trend during the overlapping period.

The time-mean MOC during the overlapping period of 17.6 ± 0.7 Sv for OFES, 19.9 ± 1.0 Sv for GLORYS, 15.9 ± 1.0 Sv for MOM6-MERRA2, and 20.4 ± 4.7 Sv for CMIP6-mean, do not significantly differ from the results obtained using AX18-XBT data (19.3 ± 2.7 Sv), except MOM6-JRA that presents a slightly weaker MOC of 15.4 ± 0.6 Sv (Figure 4b and Table 4). During the overlapping period, the time series of MOC (Figure 4b) and their trends, measured at 95% confidence intervals (Table 4), show a strengthening trend in MOC for OFES, MOM6-JRA, MOM6-MERRA2, and CMIP6-mean, which agrees with the trend obtained from AX18-XBT data.

Table 4
Mean Without Considering Seasonal Variability, Trends, and 95% Confidence Intervals (CI) for M_{ov} (Sv), MOC (Sv), and MHT (PW) From AX18-XBT Derived Data and Numerical Model Data at Nominally 34.5°S in the South Atlantic for Two Periods: Full Record Length (OFES: 1980–2017, GLORYS: 1993–2019, MOM6-JRA: 1988–2017, MOM6-MERRA2: 1982–2020, CMIP6-Mean: 1850–2014) and the Overlapping Period (2004–2014)

Meridional transports			AX18-XBT	OFES	GLORYS	MOM6-JRA	MOM6-MERRA2	CMIP6-mean
M_{ov}	Mean (Sv)	Full record length	−0.15 ± 0.09	−0.13 ± 0.04	−0.02 ± 0.03	−0.11 ± 0.02	−0.05 ± 0.03	0.05 ± 0.14
		2004–2014	−0.16 ± 0.09	−0.11 ± 0.04	−0.03 ± 0.02	−0.09 ± 0.02	−0.03 ± 0.02	0.06 ± 0.15
	Trends and 95% CI (Sv/year)	Full record length	0.0033 ± 0.0049	0.0028 ± 0.0008	−0.0018 ± 0.0011	0.0017 ± 0.0008	0.0006 ± 0.0005	0.0002 ± 0.0000
		2004–2014	0.0053 ± 0.0091	0.0048 ± 0.0050	0.0007 ± 0.0042	0.0014 ± 0.0026	0.0034 ± 0.0017	−0.0012 ± 0.0011
MOC	Mean (Sv)	Full record length	19.6 ± 2.9	17.4 ± 1.1	20.3 ± 1.1	15.8 ± 0.9	16.4 ± 0.9	19.9 ± 4.7
		2004–2014	19.3 ± 2.7	17.6 ± 0.7	19.9 ± 1.0	15.4 ± 0.6	15.9 ± 1.0	20.4 ± 4.7
	Trends and 95% CI (Sv/year)	Full record length	0.1713 ± 0.1589	0.0517 ± 0.0328	−0.0888 ± 0.0557	−0.0187 ± 0.0397	−0.0107 ± 0.0270	0.0067 ± 0.0016
		2004–2014	0.1677 ± 0.2789	0.0679 ± 0.2226	−0.1742 ± 0.2008	0.0203 ± 0.1162	0.1471 ± 0.1058	0.0024 ± 0.1011
MHT	Mean (PW)	Full record length	0.59 ± 0.16	0.58 ± 0.06	0.45 ± 0.05	0.41 ± 0.04	0.33 ± 0.04	0.55 ± 0.25
		2004–2014	0.59 ± 0.16	0.57 ± 0.06	0.45 ± 0.05	0.40 ± 0.04	0.35 ± 0.04	0.59 ± 0.25
	Trends and 95% CI (PW/year)	Full record length	0.0034 ± 0.0090	−0.0009 ± 0.0010	−0.0024 ± 0.0031	−0.0009 ± 0.0023	0.0011 ± 0.0016	0.0004 ± 0.0001
		2004–2014	0.0015 ± 0.0168	−0.0042 ± 0.0045	−0.0077 ± 0.0114	−0.0008 ± 0.0070	−0.0022 ± 0.0058	−0.0001 ± 0.0076

Note. Trends are given in units of Sv/year for M_{ov} and MOC, and in PW/year for MHT.

In contrast, GLORYS suggests a weakening trend in MOC. Among these results, the only significant trend in MOC is observed for MOM6-MERRA during the overlapping period.

Additionally, the time-mean MHT of 0.57 ± 0.06 PW for OFES, 0.45 ± 0.05 PW for GLORYS, 0.40 ± 0.04 PW for MOM6-JRA, and 0.59 ± 0.25 PW for CMIP6-mean, do not significantly differ from the results estimated using AX18-XBT data (0.59 ± 0.16 Sv), except MOM6-MERRA2 presenting a slightly weaker MHT of 0.35 ± 0.04 PW (Figure 4c and Table 4). However, during the overlapping period, when we examine the time series of MHT (Figure 4c) and their trends, measured at 95% confidence intervals, there is a discrepancy between numerical models and AX18-XBT data: the numerical models indicate a weakening trend instead of the strengthening trend shown by AX18-XBT data (Table 4). It's important to note that none of these trends are statistically significant.

3.4. M_{ov} in CGCMs Data

To understand the disagreement between the CMIP6-mean M_{ov} and the other estimates, we examined the individual time-mean M_{ov} values from each of the 32 CMIP6 historical simulations for the periods 1850–2014 (Figure 5a) and 2004–2014 (Figure 5b). We have found that only 12 out of 32 CMIP6 models present a negative sign for M_{ov} in both periods (Figures 5a and 5b), with seven of them showing a M_{ov} mean not significantly different from the AX18-XBT M_{ov} mean for the same period (2004–2014) (Figure 5b).

Next, to clarify the causes of the opposite sign of the M_{ov}, we have analyzed the different patterns in the vertical profiles of salinity, temperature, and meridional velocity across 34.5°S from the 32 CMIP6 models (Figure 6). Our results show differences in salinity and velocity profiles, but only the salinity profiles exhibit a clear separation between models with positive and negative M_{ov}. Specifically, models with positive M_{ov} have clearly fresher upper and saltier deep waters compared to those with negative M_{ov} (Figure 6). This result is consistent with previous results from CMIP4 (Liu et al., 2014) and CMIP5 (Liu et al., 2017) models.

When comparing the profiles of salinity with observations (Figure 6a), the observed data show saltier surface and fresher intermediate waters, more closely resembling the CMIP6 models with negative and positive M_{ov}, respectively. The salinity in the deep waters resembles the mean of the CMIP6 models with negative M_{ov}. Therefore, these findings suggest an alternate correspondence between observed and simulated salinity profiles in different water layers.

3.5. Covariability of the Meridional Fluxes

The results presented in Table 5 demonstrate that, from the full record length of all data sets used in this study, there is a consistent positive correlation in magnitude between the variability of MOC and M_{ov} and MHT and M_{ov},

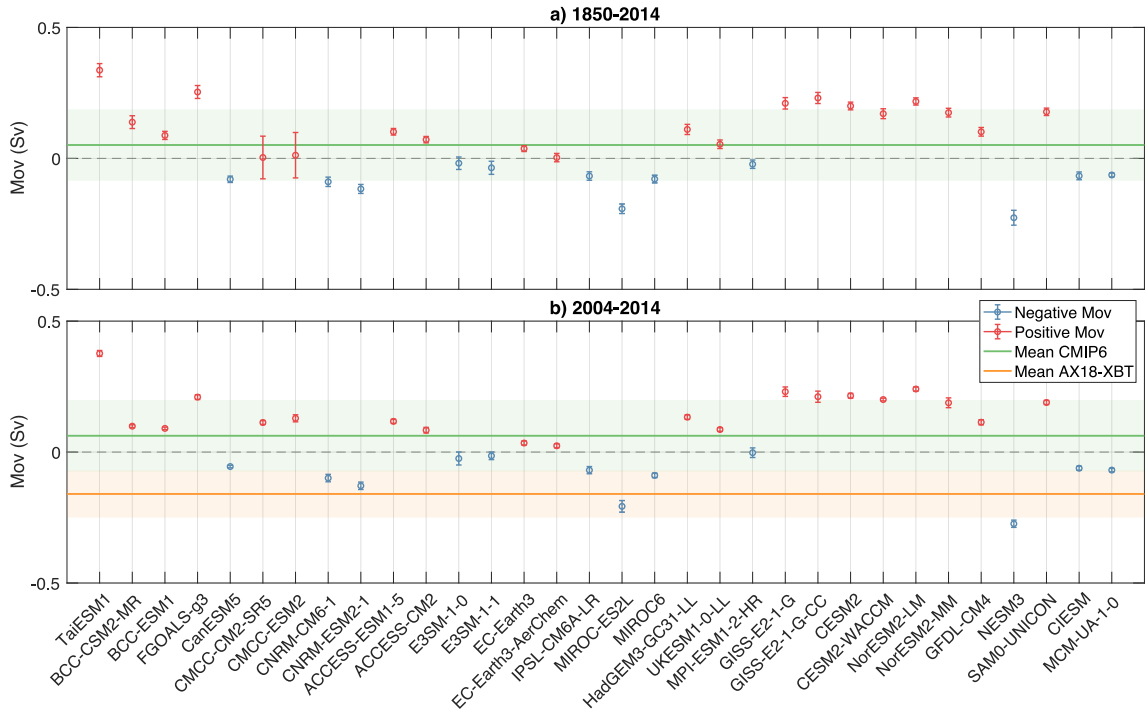

Figure 5. M_{ov} across 34.5°S in the Atlantic Ocean, employing historical data from 32 CMIP6 models for the periods (a) 1850–2014 and (b) 2004–2014. Circles and error bars indicate the mean and the standard deviation of the models without considering seasonal variability, using blue and red error bars to indicate a positive or negative model mean of M_{ov}, respectively. The green solid line represents the multi-model CMIP6 M_{ov} mean with light green shading for standard deviation in both periods (a and b). The orange solid line indicates the AX18-XBT M_{ov} mean with light orange shading for standard deviation for the period 2004–2014 (b).

as well as a positively correlated variability of MOC and MHT. Our analysis reveals different degrees of relationships between the South Atlantic meridional fluxes at 34.5°S. Starting with the relationship between MOC and M_{ov}, the analysis of AX18-XBT data a weak linear relationship, with the MOC explaining only 3% of the M_{ov} variance with a linear regression slope of approximately −0.0050 ± 0.0043 Sv/Sv (positively correlated in magnitude). However, it is important to remember that there are only 49 AX18-XBT realizations. When using the Argo data sets, a stronger linear relationship is observed, with the MOC explaining 59%–76% of the M_{ov} variance and linear regression slopes of about −0.0149 ± 0.0007 Sv/Sv (Argo Alt.) and −0.0123 ± 0.0005 Sv/Sv (RG Argo). Additionally, analyses using numerical models also show a moderately strong linear relationship between MOC and M_{ov}, explaining 30%–74% of the variance, with regression slopes ranging from −0.0091 to −0.0195 Sv/Sv.

Our analysis of AX18-XBT data shows a weak linear relationship between MHT and M_{ov}, with the MHT explaining only 17% of the M_{ov} variance and a linear regression slope of approximately −0.2310 ± 0.0733 Sv/PW (positively correlated in magnitude). The linear relationship between MHT and M_{ov} is stronger in the Argo data sets, where the MHT explains 74%–82% of the M_{ov} variance, with linear regression slopes of −0.2750 ± 0.0087 Sv/PW (Argo Alt.) and −0.4383 ± 0.0141 Sv/PW (RG Argo). Likewise, all of the numerical models exhibit a strong linear relationship between MHT and M_{ov}, explaining 61%–76% of the variance, with linear regression slopes ranging from −0.1265 to −0.3527 Sv/PW.

As expected from previous studies, there is a moderately strong relationship between the MOC and MHT in the AX18-XBT data. The MOC explains 56% of the MHT variance, with a linear regression slope of about 0.0407 ± 0.0053 PW/Sv (positively correlated). The linear relationship between the MOC and MHT is even stronger in the Argo data sets, where the MOC explains 85%–93% of the MHT variance, with linear regression slopes of 0.0557 ± 0.0013 PW/Sv (Argo Alt.) and 0.0484 ± 0.0009 PW/Sv (RG Argo). Similarly, all of the numerical models exhibit a strong linear relationship between MOC and MHT, explaining 76%–94% of the variance, with linear regression slopes ranging from 0.0483 to 0.0738 PW/Sv.

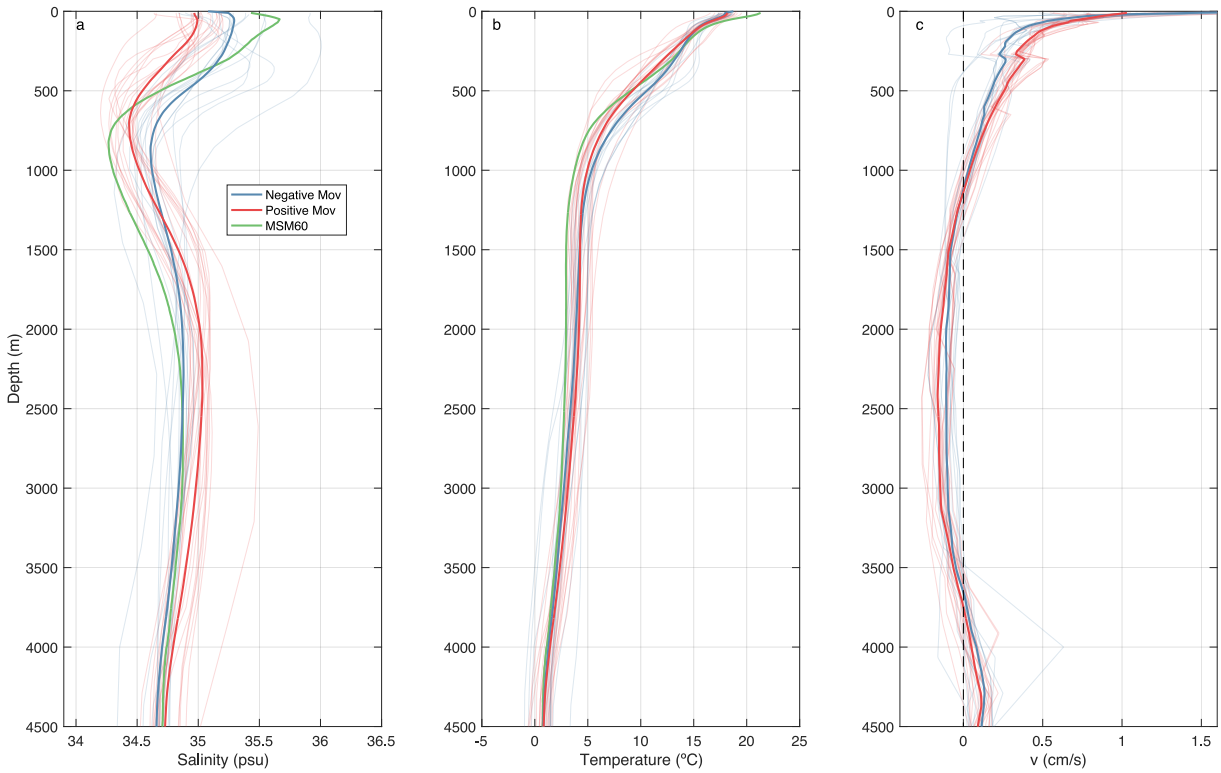

Figure 6. Time- and zonal-averages of vertical profiles of (a) salinity, (b) temperature, and (c) meridional velocity for the 32 CMIP6 models across 34.5°S. Light blue and red colors indicate positive and negative model mean of M_{ov}, respectively, while solid blue/red lines represent the mean of the models with negative/positive M_{ov}. The green solid line represents the hydrographic profiles of (a) salinity and (b) temperature from MSM60 at 34.5°S for reference.

In summary, our analysis reveals a modest linear (positively correlated in magnitude) relationship between MOC and M_{ov}, a stronger linear (positively correlated in magnitude) dependence between MHT and M_{ov}, and an even stronger linear relationship (positively correlated) between MOC and MHT derived from the data sets used. Most of the correlations exhibit moderately high R^2 values, indicating a linear relationship between these South Atlantic meridional fluxes at 34.5°S (Table 5), suggesting that an increase in M_{ov} corresponds to an increase in MOC and MHT. The strengthened MOC increases the northward transport of warm surface waters, thereby increasing MHT (positively correlated). Conversely, the positively correlated M_{ov}/MOC relationship in magnitude takes into account that a weakening of MOC reduces the transport of salty surface waters from the South Atlantic to the

Table 5
Correlation Between the South Atlantic Meridional Fluxes at 34.5°S From the Full Record Length of Observational and Model-Based Data

	M_{ov}/MOC (Sv/Sv)		M_{ov}/MHT (Sv/PW)		MHT/MOC (PW/Sv)	
Data	Slope	R^2	Slope	R^2	Slope	R^2
AX18-XBT	−0.0050 ± 0.0043	0.03	−0.2310 ± 0.0733	0.17	0.0407 ± 0.0053	0.56
Argo Alt.	−0.0149 ± 0.0007	0.59	−0.2750 ± 0.0087	0.74	0.0557 ± 0.0013	0.85
RG Argo	−0.0123 ± 0.0005	0.76	−0.4383 ± 0.0141	0.82	0.0484 ± 0.0009	0.93
OFES	−0.0174 ± 0.0002	0.52	−0.3527 ± 0.0111	0.69	0.0604 ± 0.0003	0.87
GLORYS	−0.0106 ± 0.0009	0.30	−0.3061 ± 0.0126	0.65	0.0483 ± 0.0015	0.76
MOM6-JRA	−0.0195 ± 0.0006	0.74	−0.3245 ± 0.0095	0.76	0.0560 ± 0.0009	0.92
MOM6-MERRA2	−0.0124 ± 0.0007	0.38	−0.2914 ± 0.0110	0.61	0.0525 ± 0.0011	0.83
CMIP6-mean	−0.0091 ± 0.0002	0.57	−0.1265 ± 0.0022	0.63	0.0738 ± 0.0004	0.94

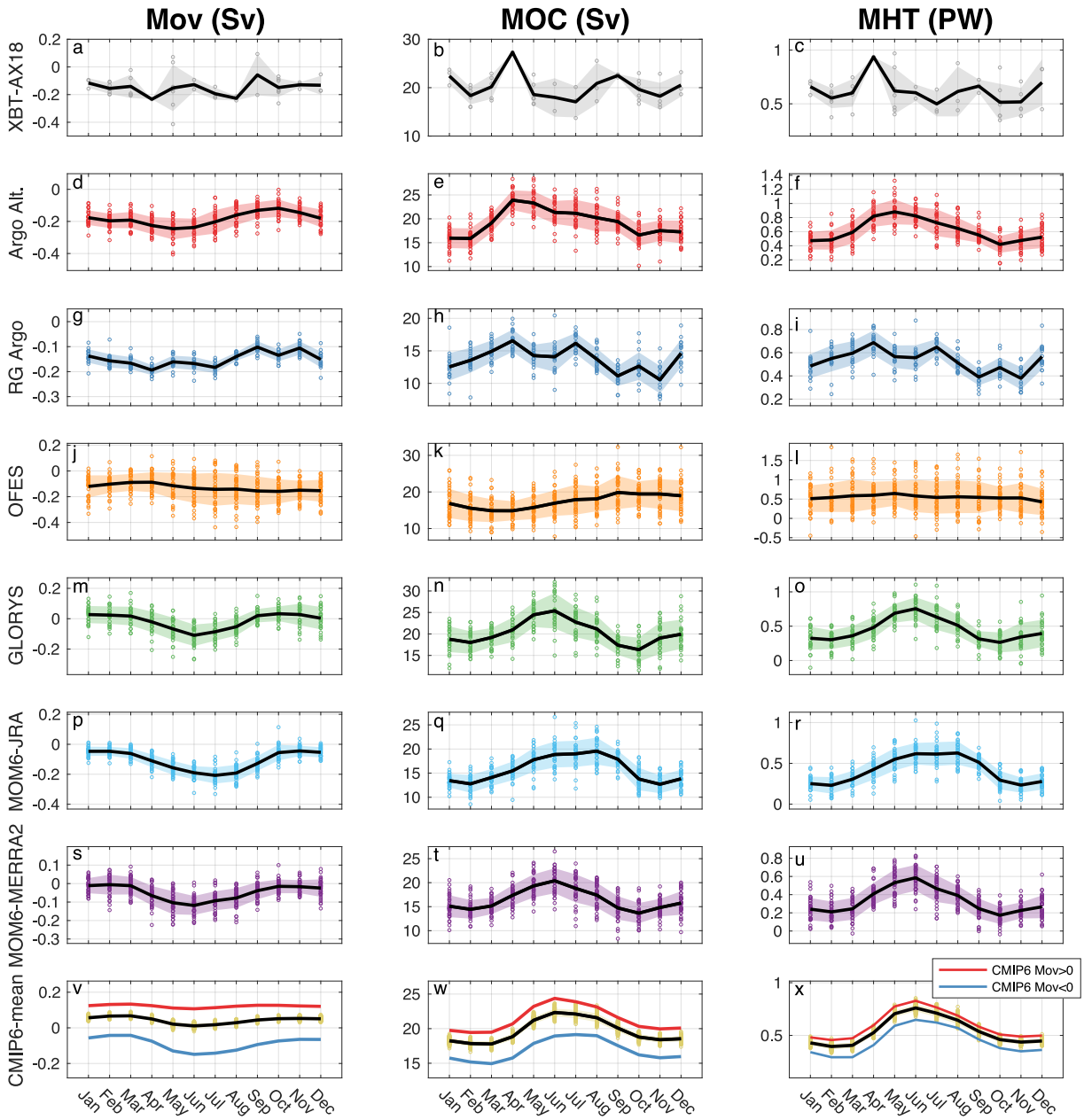

Figure 7. Seasonal variability of M_{ov} (Sv), MOC (Sv), and MHT (PW) derived from the full record length of observational and numerical model data across 34.5°S in the Atlantic Ocean for the different data sets indicated on the *y*-axis. The circles correspond to the meridional flux values for each month in the period of the corresponding data set. The black solid line connects the mean meridional flux value for each month, averaged by the different years with the standard deviation of each month included in a light color. The data sets used are AX18-XBT (a–c), Argo Alt. (d–f), RG Argo (g–i), OFES (j–l), GLORYS (m–o), MOM6-JRA (p–r), MOM6-MERRA2 (s–), and CMIP6-mean (v–x), we have also included the mean values of the CMIP6 models that estimate $M_{ov} > 0$ in red and $M_{ov} < 0$ in blue.

North Atlantic. This reduction contributes to the accumulation of freshwater and lighter surface waters in the subpolar North Atlantic, hindering the sinking process and further contributing to AMOC weakening.

3.6. Seasonal Variability of the Meridional Fluxes

Figure 7 illustrates the seasonal variability of M_{ov} (first column), MOC (second column), and MHT (third column) in the Atlantic Ocean at nominally 34.5°S using observational and numerical model data. It is worth noticing the difficulty in inferring the seasonal variability of the South Atlantic meridional fluxes with the AX18-XBT data due to their limited sample size for some months (only February, March, May, October, and November

have more than four samples) (Figures 7a–7c). OFES does not show strong seasonal variability in any of the South Atlantic meridional fluxes (Figures 7j–7l). The other data sets have similar seasonal cycles for M_{ov}, MOC, and MHT, with stronger negative M_{ov} values and stronger positive MOC and MHT values observed during late austral autumn and winter months, specifically from April to August.

These findings support the previously described covariability between the South Atlantic meridional fluxes discussed in Section 3.4. Note that the CMIP6-mean M_{ov} values remain positive throughout most of the year. However, when we examine the average seasonal variability of the CMIP6 models with positive M_{ov} (20 CMIP6 models) versus those with negative M_{ov} mean (12 CMIP6 models), the results indicate that M_{ov} exhibits stronger seasonal variability for CMIP6 models with $M_{ov} < 0$. Additionally, on average the CMIP6 models with a positive M_{ov} mean have stronger MOC and MHT values during all months.

4. Discussion and Conclusions

In this study, we use high-density AX18-XBT data along with Argo float-derived data sets and numerical model data to conduct a multi-data set analysis of M_{ov}, as well as MOC and MHT in the South Atlantic Ocean at 34.5°S. Through our updated AX18-XBT data analysis, an 18-year time series of the South Atlantic meridional fluxes is generated, which are then compared with data from Argo Alt., RG Argo, OFES, GLORYS, MOM6-JRA, MOM6-MERRA2, and 32 CMIP6 models. Our comparison is aimed at determining the consistency between the observational and modeling data in the South Atlantic region, as well as investigating the correlation and seasonal variability of the South Atlantic meridional fluxes.

The stability of the MOC is assessed in this study by estimating the meridional freshwater flux (M_{ov}) at 34.5°S in the Atlantic Ocean. This flux is crucial in determining the basin-scale MOC salt feedback because it regulates the amount of freshwater entering the basin, thereby influencing the salt concentration and density of the water. The M_{ov} results obtained during the overlapping period from AX18-XBT sections, as well as from monthly data of Argo Alt., RG Argo, OFES, MOM6-JRA, and CMIP6-mean are not significantly different. However, GLORYS and MOM6-MERRA present lower M_{ov} negative values. The observations consistently show a negative M_{ov} with a mean value from AX18-XBT of -0.16 ± 0.09 Sv, as well as the other mean estimates of [−0.03 to −0.18] from Argo float-derived data and OGCMs. In contrast, only the CMIP6 ensemble has a positive M_{ov} with a mean value of 0.06 ± 0.15 Sv. The negative M_{ov} values observed at approximately 34.5°S in the Atlantic Ocean indicate that the AMOC transports freshwater toward the south, which requires a net inflow of freshwater north of 34.5°S to maintain the salinity associated with the overturning circulation. Therefore, our study suggests that the AMOC is currently in a bistable regime and could collapse if a large enough freshwater perturbation occurs (Rahmstorf, 1996). In addition to freshwater perturbation, Liu et al. (2017) showed that the bistable AMOC can collapse under double CO_2 warming. Our XBT-derived mean is consistent with prior studies that employed observational data to demonstrate the export of freshwater [−0.08 to −0.34 Sv] from the Atlantic Ocean through its southern boundary by the overturning circulation Bryden et al. (2011), McDonagh & King (2005), Garzoli et al. (2013), Caínzos et al. (2022), Weijer et al. (1999), and Huisman et al. (2010). In contrast, Caínzos et al. (2022) estimated from observations an inconclusive M_{ov} result of 0.0 ± 0.02 Sv, hence indicating that the AMOC is not exporting enough freshwater from the Atlantic Ocean. As mentioned, the negative M_{ov} derived from AX18-XBT data differs from the CMIP6-mean results providing $M_{ov} > 0$. This $M_{ov} > 0$ CMIP6-mean result agrees with previous model-based estimates in the South Atlantic of [0.09–0.18 Sv] by Drijfhout et al. (2011)and Mecking et al. (2017), as well as from a range of 0.24 to −0.11 Sv at 33°S estimated by de Vries and Weber (2005). In addition, our study analyzed trends in M_{ov}, measured at 95% confidence intervals, and found a positive (decreasing) trend during the overlapping period in all models except the multi-model CMIP6-mean. It is important to note that the interannual variability is highly dependent on the data set and period used, mostly exhibiting non-significant trends during the overlapping period. Therefore, based on the trends measured at 95% confidence intervals from the data sets used in our study, we cannot definitively determine whether the M_{ov} has been decreasing or increasing its negative value over time.

We find that only 12 out of 32 CMIP6 models exhibited a negative M_{ov} mean value. It is well-known that there is a positive salinity bias in several current generations of CGCMs at nominally 34.5°S in the South Atlantic Ocean, as found using data from CMIP3 models by Liu et al. (2014), CMIP4 models by Mecking et al. (2017), and CMIP5 models by Weijer et al. (2019) and Liu et al. (2017) in the same region. Our analysis of vertical salinity profiles has identified a clear differentiation between CMIP6 models presenting positive and negative M_{ov} values. Models

with positive M_{ov} values have fresher upper and saltier deep waters than those with negative M_{ov} values, suggesting that the salinity structure may play a role in determining the sign of M_{ov}. We have attempted to understand the differences among these models by conducting calculations in three specific sections (a zonal section at 34.5°S, and two meridional sections at Drake Passage and south of South Africa). These calculations included computing the freshwater flux through each section, the evaporation minus precipitation within the enclosed region, and the overall salinity transport and its divergence (not shown). Despite our efforts, we have not identified any specific patterns or behaviors in the respective fluxes that can explain the differences in M_{ov}'s sign.

We have estimated that the strength of MOC at nominally 34.5°S, using AX18-XBT data during the overlapping period (2004–2014), is 19.3 ± 2.7 Sv. This value is consistent with our mean estimates of [15.9–20.4 Sv] using Argo Alt., OFES, GLORYS, MOM6-MERRA2, and CMIP6-mean data sets. Nevertheless, we have estimated a slightly weaker MOC of 15.4 ± 0.6 Sv from MOM6-JRA, and a significantly weaker MOC of 13.4 ± 0.4 Sv when using RG Argo data compared to the AX18-XBT result. Our estimate of the strength of MOC at nominally 34.5°S using AX18-XBT data is also consistent with previous observational and model estimates of [14.7–20.7 Sv] by Manta et al. (2021), Kersalé et al. (2021), Meinen et al. (2018), Perez et al. (2011), Dong et al. (2011, 2015), Majumder et al. (2016), and Garzoli et al. (2013), as well as Weijer et al. (2020). However, our AX18-XBT mean result shows a stronger MOC than the 14.8 ± 1.0 Sv estimated by Arumí-Planas et al. (2023).

The significantly weaker MOC estimated with RG Argo compared to AX18-XBT data could be explained by the absence of Argo data in the regions shallower than 2,000 m depth near the east and west coasts, as well as the uneven distribution of Argo data in space and time. Argo floats provide discrete profiles at specific locations and times, which can introduce sampling errors when interpolated. Additionally, Argo float data may have biases in the measurements of ocean properties, such as temperature and salinity, that can affect the estimation of transports (Roemmich & Gilson, 2009). However, this is not the case with the Argo Alt. product, which combines temperature and salinity profiles from Argo floats with monthly satellite altimetry SLA, reducing the underestimation of MOC.

Our estimate of MHT from the AX18-XBT transect data, which is 0.59 ± 0.16 PW, establishes that the South Atlantic Ocean transports heat northward. This result is consistent with mean MHT estimates of [0.40–0.62 PW] from Argo Alt., RG Argo, OFES, GLORYS, MOM6-JRA, and CMIP6-mean. However, MOM6-MERRA presents a lower MHT of 0.35 ± 0.04 PW compared to the AX18-XBT result. These findings align with previously published observational studies, presenting [0.49–0.55 PW] by Garzoli & Baringer (2007), Dong et al. (2009, 2015), Garzoli et al. (2013), and Kersalé et al. (2021), as well as previous studies using numerical model data of [0.38 PW to 0.42 PW] by Perez et al. (2011) and Dong et al. (2011). Therefore, our estimates of MOC and MHT are consistent with earlier estimates obtained by models and observations in the South Atlantic at 34.5°S, demonstrating the robustness of those earlier estimates of MOC strength of ≈19 Sv and northward MHT of ≈0.60 PW. We have also analyzed time series trends measured at 95% confidence intervals and found that MOC and MHT have been strengthening using AX18-XBT data for both the full data set period and the overlapping period. While OFES, MOM6-JRA, MOM6-MERRA2, and CMIP6-mean show strengthening trends in MOC during the overlapping period, which agrees with the AX18-XBT data, Argo Alt., RG Argo and GLORYS suggest a weakening, consistent with RAPID array's findings at 26°N (Frajka-Williams et al., 2019). However, Frajka-Williams et al. (2019) reported different trends across latitudes in the Atlantic Ocean from 2004 to 2017, noting strengthening and weakening trends in MOC at 16°N and 26°N, respectively. The study highlighted latitudinal dependence in AMOC variability and suggests that comparisons between results at 34.5°S and 26°N are challenging. It's essential to emphasize that, among these data sets, only MOM6-MERRA presents a significant trend in MOC during the overlapping period. For MHT, Argo data sets, OGCMs, and CGCMs indicate a non-significant weakening trend during the overlapping period instead of the strengthening MHT obtained using AX18-XBT data.

Based on our estimates, we have examined the correlation between M_{ov}/MOC, M_{ov}/MHT, and MHT/MOC across 34.5°S in the South Atlantic Ocean. We found a linear relationship between the variability of these South Atlantic meridional fluxes, estimating a negative linear regression slope between M_{ov}/MOC and M_{ov}/MHT (positively correlated in magnitude), and a positive slope between MHT/MOC (positively correlated). Our analysis reveals different degrees of relationships between MOC and M_{ov}: AX18-XBT data shows a weak linear relationship, explaining only 3% of the M_{ov} variance with a linear regression slope of approximately −0.0050 ± 0.0043 Sv/Sv; Argo data sets explain 59%–76% of the variance, with linear regression slopes from −0.0149 to −0.0123 Sv/Sv; and numerical models explain 30%–74% of the variance, with slopes ranging from −0.0091 to −0.0195 Sv/Sv.

Similarly, we found a linear relationship between MHT and M_{ov} with AX18-XBT data explaining only 17% of the M_{ov} variance with a linear regression slope of -0.2310 ± 0.0733 Sv/PW; Argo data sets explain 74%–82% with linear regression slopes from -0.2750 to -0.4383 Sv/PW; and numerical models explain 61%–76% of the variance, with linear regression slopes ranging from -0.1265 to -0.3527 Sv/PW. Finally, the relationship between MOC and MHT derived from the AX18-XBT data explain 56% of the MHT variance, with a slope of about 0.0407 ± 0.0053 PW/Sv; Argo data sets explain 85%–93% of the variance, with slopes of 0.0484–0.0557 PW/Sv; and numerical models explain 76%–94% of the variance, with slopes ranging from 0.0483 to 0.0738 PW/Sv. This finding is consistent with the previous results of the correlated variability between MOC and MHT with a slope of ≈0.05 PW/Sv from observations and models at nominally 34.5°S in the South Atlantic Ocean (Dong et al., 2009, 2011; Perez et al., 2011). Therefore, the linear regressions suggest that a higher M_{ov} corresponds to a higher MOC and MHT.

The positive relationship between MOC and MHT can be explained by the fact that a strengthening of MOC, which carries warm surface waters northward, results in an increase of MHT due to the associated increased transport of warm surface waters. However, the positive correlation in magnitude between MOC and M_{ov} is more complex. This relationship can be explained by the fact that as the AMOC weakens, the transport of salty surface waters from the South Atlantic to the North Atlantic decreases. Within the subpolar North Atlantic, these waters undergo cooling, densification, and subsequent sinking to deeper layers before flowing southward. Consequently, the weakened AMOC contributes to the accumulation of less saline surface waters in the subpolar North Atlantic. This reduced transport in the upper layers by the AMOC may exert an influence on the density of surface waters, hindering the sinking process in the North Atlantic and thereby exacerbating the overall weakening of the AMOC.

The lower R^2 values obtained from the AX18-XBT data may be attributed to the small sample size of the data set, as well as to the inherent limitations of the XBT data. XBTs do not directly measure salinity or velocity, which can introduce errors and limitations in capturing the complete picture of ocean circulation. Due to changes in the orientation of the shipping routes, the AX18-XBT lines are not always across fixed latitudes, which could also influence the relationships of M_{ov}/MHT with AMOC. The higher R^2 values obtained from the numerical models can be explained by the fact that these models are based on physical equations and incorporate various data sets and parameterizations, allowing them to capture complex interactions and processes that might not be fully captured by the limited observations from AX18-XBT data. This results in a stronger linear relationship between M_{ov}/MOC, M_{ov}/MHT and MHT/MOC when using numerical models.

The time series of the South Atlantic meridional fluxes exhibit significant interannual variability from all data sets used in our study. Across almost all of the observational and numerical model data sets, the seasonal cycle in M_{ov}, MOC, and MHT, vary such that there are minima in M_{ov} (largest negative values relative to the mean) and maxima in MOC and MHT (largest positive values relative to the mean) from late austral autumn to winter, specifically from April to August, which agrees with the seasonal variability previously reported by Dong et al. (2009). Nevertheless, we cannot infer the seasonal cycle from the AX18-XBT data due to limited sampling, as the transect is only sampled every 3 months, and the data for some months are limited. Specifically, we only have more than four samples available for February, March, May, October, and November. Additionally, sampling aliasing in space and time may influence the XBT data, as the mean latitude of each AX18 transect varies between 30°S and 35°S (Figure 1, Dong et al., 2014).

In conclusion, this study improves our understanding of the variability of freshwater transport by the Atlantic Meridional Overturning Circulation and its impact on the global climate system. The M_{ov} findings from observational data, ocean models, and some coupled climate models considered here suggest a bistable regime of the meridional overturning circulation according to a simple conceptual model and a global circulation model (Rahmstorf, 1996). Additionally, this study highlights the different salinity structures for CMIP6 models with positive M_{ov} mean, indicating that the salinity biases may be responsible for the opposite sign of M_{ov}. Specifically, models with positive M_{ov} values show fresher upper and deeper saltier waters compared to those estimating negative M_{ov} values. Therefore, we emphasize the need for refining CMIP6 model representations, specifically the salinity bias, to enhance the reliability of AMOC projections in CMIP6 models, especially given the significant implications for IPCC risk analyses. Finally, our results demonstrate that seasonal variability of the data sets provides a coherent picture of the concomitant variability and correlation of the South Atlantic meridional fluxes at 34.5°S: M_{ov} is positively correlated in magnitude to MOC and MHT, and MOC is positively correlated to MHT, presenting higher negative M_{ov} values and higher positive MOC/MHT transports from April to August.

Conflict of Interest

The authors declare no conflicts of interest relevant to this study.

Data Availability Statement

Additional information on AX18-XBT data for each transect line can be found at http://www.aoml.noaa.gov/phod/hdenxbt/ax_home.php. Other data sets used in this study are publicly available for download from different websites. Satellite altimetry products produced by the Copernicus Marine and Environment Monitoring Service are available at https://resources.marine.copernicus.eu/product-detail/SEALEVEL-GLO_PHY_L4_MY_008_047/INFORMATION (https://doi.org/10.48670/moi-00148). Argo Climatology data available at https://sio-argo.ucsd.edu/RG_Climatology.html which were complemented using YoMaHa data accessible at http://apdrc.soest.hawaii.edu/projects/yomaha/, GLORYS data from https://resources.marine.copernicus.eu/, MOM6-JRA data available at https://www.gfdl.noaa.gov/mom-ocean-model/, MOM6-MERRA2 output by Harrison (2022) is archived with an associated https://doi.org/10.5281/zenodo.6342240, and the 32 CMIP6 models' data can be found at https://esgf-node.llnl.gov/search/cmip6 (Bader et al., 2019a, 2019b; Bentsen et al., 2019; Boucher et al., 2018; Cao & Wang, 2019; Danabasoglu, 2019a, 2019b; Dix et al., 2019; (EC-Earth), 2019, 2020; Guo et al., 2018; Hajima et al., 2019; Huang, 2019; Jungclaus et al., 2019; Lee & Liang, 2020; Li, 2019; Lovato & Peano, 2020; Lovato et al., 2021; (NASA/GISS), 2018, 2019; Park & Shin, 2019; Ridley et al., 2019; Seferian, 2018; Seland et al., 2019; Stouffer, 2019; Swart et al., 2019; Tang et al., 2019; Tatebe & Watanabe, 2018; Voldoire, 2018; Wu et al., 2018; Zhang et al., 2018; Ziehn et al., 2019). The hydrographic data collected during the expedition of the German Research Vessel *Maria S. Merian* (MSM60) at 34.5°S can be accessed at https://doi.org/10.2312/cr_msm60. For further inquiries, please reach out to the corresponding author.

Acknowledgments

This study was supported by the SAGA (RTI2018-100844-B-C31, RTI2018-100844-B-C32 and RTI2018-100844-B-C33) and SACO (PID2022-139403NB-C21 and PID2022-139403NB-C22) projects funded by the Ministerio de Ciencia, Innovación y Universidades of the Spanish Government, and Feder. This article is a publication of the Unidad Océano y Clima from Universidad de Las Palmas de Gran Canaria, an R&D&I CSIC associate unit. This work was conducted by C. Arumí-Planas as part of her work at IOCAG, in the doctoral program in Oceanography and Global Change. C. Arumí-Planas acknowledges the Agencia Canaria de Investigación, Innovación y Sociedad de la Información (ACIISI) and the Fondo Social Europeo Plus (FSE+) Programa Operativo Integrado de Canarias 2021–2027, Eje 3 Tema Prioritario 74 (85%) grant programs of "Apoyo al personal investigador en formación" TESIS2021010028 and "Estancias Breves en España y en el Extranjero 2022" EST2022010028, as well as the NOAA Atlantic Oceanographic and Meteorological Laboratory in Miami for hosting a guest student to develop the study. S. Dong and R. Perez are supported via NOAA's Global Monitoring and Observing program (FundRef number 100007298) under the Southwest Atlantic Meridional Overturning Circulation (SAM) project, the State of Climate for the meridional heat transport project, and the AOML XBT project, with additional support from the NOAA Atlantic Oceanographic and Meteorological Laboratory.

References

Adcroft, A., Anderson, W., Balaji, V., Blanton, C., Bushuk, M., Dufour, C. O., et al. (2019). The GFDL global ocean and sea ice model OM4.0: Model description and simulation features. *Journal of Advances in Modeling Earth Systems*, *11*(10), 3167–3211. https://doi.org/10.1029/2019MS001726

Arhan, M., Mercier, H., & Park, Y.-H. (2003). On the deep water circulation of the eastern South Atlantic Ocean. *Deep Sea Research Part I: Oceanographic Research Papers*, *50*(7), 889–916. https://doi.org/10.1016/S0967-0637(03)00072-4

Arumí-Planas, C., Pérez-Hernández, M. D., Pelegrí, J. L., Vélez-Belchí, P., Emelianov, M., Caínzos, V., et al. (2023). The South Atlantic circulation between 34.5°S, 24°S and above the mid-Atlantic ridge from an inverse box model. *Journal of Geophysical Research: Oceans*, *128*(5), 1–21. https://doi.org/10.1029/2022JC019614

Bader, D. C., Leung, R., Taylor, M., & McCoy, R. B. (2019a). E3SM-Project E3SM1.0 model output prepared for CMIP6 CMIP historical (Version 20221114) [Dataset]. *Earth System Grid Federation*. https://doi.org/10.22033/ESGF/CMIP6.4497

Bader, D. C., Leung, R., Taylor, M., & McCoy, R. B. (2019b). E3SM-Project E3SM1.1 model output prepared for CMIP6 CMIP historical (Version 20221114) [Dataset]. *Earth System Grid Federation*. https://doi.org/10.22033/ESGF/CMIP6.11485

Baker, J. A., Bell, M. J., Jackson, L. C., Renshaw, R., Vallis, G. K., Watson, A. J., et al. (2023). Overturning pathways control AMOC weakening in CMIP6 models. *ESS Open Archive eprints*, https://doi.org/10.22541/essoar.167751597.72764615/v1

Baringer, M. O., & Garzoli, S. L. (2007). Meridional heat transport determined with expendable bathythermographs-Part I: Error estimates from model and hydrographic data. *Deep-Sea Research Part I Oceanographic Research Papers*, *54*(8), 1390–1401. https://doi.org/10.1016/j.dsr.2007.03.011

Bentsen, M., Oliviè, D. J. L., Seland, Ø., Toniazzo, T., Gjermundsen, A., Graff, L. S., et al. (2019). NCC NorESM2-MM model output prepared for CMIP6 CMIP historical (Version 20221116) [Dataset]. *Earth System Grid Federation*. https://doi.org/10.22033/ESGF/CMIP6.8040

Biastoch, A., Schwarzkopf, F. U., Getzlaff, K., Rühs, S., Martin, T., Scheinert, M., et al. (2021). Regional imprints of changes in the Atlantic Meridional Overturning Circulation in the eddy-rich ocean model VIKING20X. *Ocean Science*, *17*(5), 1177–1211. https://doi.org/10.5194/os-17-1177-2021

Boucher, O., Denvil, S., Levavasseur, G., Cozic, A., Caubel, A., Foujols, M.-A., et al. (2018). IPSL IPSL-CM6A-LR model output prepared for CMIP6 CMIP historical (Version 20221107) [Dataset]. *Earth System Grid Federation*. https://doi.org/10.22033/ESGF/CMIP6.5195

Bryden, H. L., & Imawaki, S. (2001). Chapter 6.1 Ocean heat transport. In G. Siedler, J. Church, & J. Gould (Eds.), *Ocean circulation & climate: Observing and modelling the global ocean* (pp. 455–474). Academic Press. https://doi.org/10.1016/S0074-6142(01)80134-0

Bryden, H. L., King, B. A., & McCarthy, G. D. (2011). South Atlantic overturning circulation at 24°S. *Journal of Marine Research*, *69*(1), 38–55. https://doi.org/10.1357/002224011798147633

Caínzos, V., Hernández-Guerra, A., McCarthy, G. D., McDonagh, E. L., Cubas Armas, M., & Pérez-Hernández, M. D. (2022). Thirty years of GOSHIP and WOCE data: Atlantic overturning of mass, heat, and freshwater transport. *Geophysical Research Letters*, *49*(4), 1–12. https://doi.org/10.1029/2021GL096527

Cao, J., & Wang, B. (2019). NUIST NESMv3 model output prepared for CMIP6 CMIP historical (Version 20221116) [Dataset]. *Earth System Grid Federation*. https://doi.org/10.22033/ESGF/CMIP6.8769

Chidichimo, M. P., Perez, R. C., Speich, S., Kersalé, M., Sprintall, J., Dong, S., et al. (2023). Energetic overturning flows, dynamic interocean exchanges, and ocean warming observed in the South Atlantic. *Communications Earth and Environment*, *4*, 10. https://doi.org/10.1038/s43247-022-00644-x

Cimatoribus, A. A., Drijfhout, S. S., den Toom, M., & Dijkstra, H. A. (2012). Sensitivity of the Atlantic meridional overturning circulation to South Atlantic freshwater anomalies. *Climate Dynamics*, *39*(9–10), 2291–2306. https://doi.org/10.1007/s00382-012-1292-5

Danabasoglu, G. (2019a). NCAR CESM2 model output prepared for CMIP6 CMIP historical (Version 20221103) [Dataset]. *Earth System Grid Federation*. https://doi.org/10.22033/ESGF/CMIP6.7627

Danabasoglu, G. (2019b). NCAR CESM2-WACCM model output prepared for CMIP6 CMIP historical (Version 20221109) [Dataset]. *Earth System Grid Federation*. https://doi.org/10.22033/ESGF/CMIP6.10071

de Vries, P., & Weber, S. L. (2005). The Atlantic freshwater budget as a diagnostic for the existence of a stable shut down of the meridional overturning circulation. *Geophysical Research Letters*, *32*(9), 1–4. https://doi.org/10.1029/2004GL021450

Dijkstra, H. A. (2007). Characterization of the multiple equilibria regime in a global ocean model. *Tellus, Series A: Dynamic Meteorology and Oceanography*, *59*(5), 695–705. https://doi.org/10.1111/j.1600-0870.2007.00267.x

Dix, M., Bi, D., Dobrohotoff, P., Fiedler, R., Harman, I., Law, R., et al. (2019). CSIRO-ARCCSS ACCESS-CM2 model output prepared for CMIP6 CMIP historical (Version 20221106) [Dataset]. *Earth System Grid Federation*. https://doi.org/10.22033/ESGF/CMIP6.4271

Dong, S., Baringer, M. O., Goni, G. J., Meinen, C. S., & Garzoli, S. L. (2014). Seasonal variations in the South Atlantic meridional overturning circulation from observations and numerical models. *Geophysical Research Letters*, *41*(13), 4611–4618. https://doi.org/10.1002/2014GL060428

Dong, S., Garzoli, S., & Baringer, M. (2011). The role of interocean exchanges on decadal variations of the meridional heat transport in the South Atlantic. *Journal of Physical Oceanography*, *41*(8), 1498–1511. https://doi.org/10.1175/2011JPO4549.1

Dong, S., Garzoli, S., Baringer, M., Meinen, C., & Goni, G. (2009). Interannual variations in the Atlantic meridional overturning circulation and its relationship with the net northward heat transport in the South Atlantic. *Geophysical Research Letters*, *36*(20), L20606. https://doi.org/10.1029/2009GL039356

Dong, S., Goni, G., & Bringas, F. (2015). Temporal variability of the South Atlantic meridional overturning circulation between 20°S and 35°S. *Geophysical Research Letters*, *42*(18), 7655–7662. https://doi.org/10.1002/2015GL065603

Dong, S., Goni, G., Domingues, R., Bringas, F., Goes, M., Christophersen, J., & Baringer, M. (2021). Synergy of in situ and satellite ocean observations in determining meridional heat transport in the Atlantic Ocean. *Journal of Geophysical Research: Oceans*, *126*(4). https://doi.org/10.1029/2020JC017073

Drévillon, M., Bahurel, P., Bazin, D., Benkiran, M., Beuvier, J., Crosnier, L., et al. (2018). Learning about copernicus marine environment monitoring Service "CMEMS": A practical introduction to the use of the European operational Oceanography Service. In *New frontiers in operational oceanography*. In *GODAE OceanView*. https://doi.org/10.17125/gov2018.ch25

Drijfhout, S. S., Weber, S. L., & van der Swaluw, E. (2011). The stability of the MOC as diagnosed from model projections for pre-industrial, present and future climates. *Climate Dynamics*, *37*(7–8), 1575–1586. https://doi.org/10.1007/s00382-010-0930-z

(EC-Earth), E.-E. C. (2019). EC-Earth-Consortium EC-Earth3 model output prepared for CMIP6 CMIP historical (Version 20221115) [Dataset]. *Earth System Grid Federation*. https://doi.org/10.22033/ESGF/CMIP6.4700

(EC-Earth), E.-E. C. (2020). EC-Earth-Consortium EC-Earth3-AerChem model output prepared for CMIP6 CMIP historical (Version 20221115) [Dataset]. *Earth System Grid Federation*. https://doi.org/10.22033/ESGF/CMIP6.4701

Frajka-Williams, E., Ansorge, I. J., Baehr, J., Bryden, H. L., Chidichimo, M. P., Cunningham, S. A., et al. (2019). Atlantic meridional overturning circulation: Observed transport and variability. *Frontiers in Marine Science*, *6*(JUN), 1–18. https://doi.org/10.3389/fmars.2019.00260

Ganachaud, A., & Wunsch, C. (2000). Improved estimates of global ocean circulation, heat transport and mixing from hydrographic data. *Nature*, *408*(6811), 453–457. https://doi.org/10.1038/35044048

Garcia, H. E., Weathers, K. W., Paver, C. R., Smolyar, I., Boyer, T. P., Locarnini, M. M., et al. (2019). In A. Mishonov Technical Editor (Eds.), *World Ocean Atlas 2018. Vol. 4: Dissolved inorganic nutrients (phosphate, nitrate and nitrate+nitrite, silicate)* Ref. NOAA Atlas NESDIS (Vol. 84, p. 35). https://archimer.ifremer.fr/doc/00651/76336/

Garzoli, S. L., & Baringer, M. O. (2007). Meridional heat transport determined with expandable bathythermographs-Part II: South Atlantic transport. *Deep-Sea Research Part I Oceanographic Research Papers*, *54*(8), 1402–1420. https://doi.org/10.1016/j.dsr.2007.04.013

Garzoli, S. L., Baringer, M. O., Dong, S., Perez, R. C., & Yao, Q. (2013). South Atlantic meridional fluxes. *Deep Sea Research Part I: Oceanographic Research Papers*, *71*, 21–32. https://doi.org/10.1016/j.dsr.2012.09.003

Gent, P. R. (2018). A commentary on the Atlantic meridional overturning circulation stability in climate models. *Ocean Modelling*, *122*, 57–66. https://doi.org/10.1016/j.ocemod.2017.12.006

Goes, M., Christophersen, J., Dong, S., Goni, G., & Baringer, M. O. (2018). An updated estimate of salinity for the Atlantic Ocean sector using temperature–salinity relationships. *Journal of Atmospheric and Oceanic Technology*, *35*(9), 1771–1784. https://doi.org/10.1175/JTECH-D-18-0029.1

Guo, H., John, J. G., Blanton, C., McHugh, C., Nikonov, S., Radhakrishnan, A., et al. (2018). NOAA-GFDL GFDL-CM4 model output historical (Version 20221107) [Dataset]. *Earth System Grid Federation*. https://doi.org/10.22033/ESGF/CMIP6.8594

Hajima, T., Abe, M., Arakawa, O., Suzuki, T., Komuro, Y., Ogura, T., et al. (2019). MIROC MIROC-ES2L model output prepared for CMIP6 CMIP historical (Version 20221107) [Dataset]. *Earth System Grid Federation*. https://doi.org/10.22033/ESGF/CMIP6.5602

Harrison, M. (2022). MJHarrison-GFDL/Harrison_JAMES_2021: v1.0.0 (v1.0.0) [Dataset]. *Zenodo*. https://doi.org/10.5281/zenodo.6342240

Harrison, M., Adcroft, A., Hallberg, R., & Sergienko, O. (2022). Improved surface mass balance closure in ocean hindcast simulations. *Journal of Advances in Modeling Earth Systems*, *14*(7). https://doi.org/10.1029/2021MS002888

Hernández-Guerra, A., Machín, F., Antoranz, A., Cisneros-Aguirre, J., Gordo, C., Marrero-Díaz, A., et al. (2002). Temporal variability of mass transport in the Canary Current. *Deep Sea Research Part II: Topical Studies in Oceanography*, *49*(17), 3415–3426. https://doi.org/10.1016/S0967-0645(02)00092-9

Hernández-Guerra, A., Talley, L. D., Pelegrí, J. L., Vélez-Belchí, P., Baringer, M. O., Macdonald, A. M., & McDonagh, E. L. (2019). The upper, deep, abyssal and overturning circulation in the Atlantic Ocean at 30°S in 2003 and 2011. *Progress in Oceanography*, *176*, 102136. https://doi.org/10.1016/j.pocean.2019.102136

Huang, W. (2019). THU CIESM model output prepared for CMIP6 CMIP historical (Version 20221116) [Dataset]. *Earth System Grid Federation*. https://doi.org/10.22033/ESGF/CMIP6.8843

Huisman, S. E., Toom, M. D., Dijkstra, H. A., & Drijfhout, S. (2010). An indicator of the multiple equilibria regime of the Atlantic meridional overturning circulation. *Journal of Physical Oceanography*, *40*(3), 551–567. https://doi.org/10.1175/2009JPO4215.1

Jackson, L. C., Kahana, R., Graham, T., Ringer, M. A., Woollings, T., Mecking, J. V., & Wood, R. A. (2015). Global and European climate impacts of a slowdown of the AMOC in a high resolution GCM. *Climate Dynamics*, *45*(11–12), 3299–3316. https://doi.org/10.1007/s00382-015-2540-2

Jungclaus, J., Bittner, M., Wieners, K.-H., Wachsmann, F., Schupfner, M., Legutke, S., et al. (2019). MPI-M MPI-ESM1.2-HR model output prepared for CMIP6 CMIP historical (Version 20221114) [Dataset]. *Earth System Grid Federation*. https://doi.org/10.22033/ESGF/CMIP6.6594

Keller, K., Tan, K., Morel, F. M., & Bradford, D. F. (2000). Preserving the ocean circulation: Implications for climate policy. *Climatic Change*, *47*(1), 17–43. https://doi.org/10.3386/w7476

Kersalé, M., Meinen, C. S., Perez, R. C., Piola, A. R., Speich, S., Campos, E. J. D., et al. (2021). Multi-year estimates of daily heat transport by the atlantic meridional overturning circulation at 34.5°S. *Journal of Geophysical Research: Oceans*, *126*(5), 1–23. https://doi.org/10.1029/2020JC016947

Lebedev, K., Yoshinari, H., Maximenko, N. A., & Hacker, P. W. (2007). YoMaHa'07: Velocity data assessed from trajectories of Argo floats at parking level and at the sea surface. *IPRC Technical Note No.*, *4*(2), 16.

Lee, W.-L., & Liang, H.-C. (2020). AS-RCEC TaiESM1.0 model output prepared for CMIP6 CMIP historical (Version 20221116) [Dataset]. *Earth System Grid Federation*. https://doi.org/10.22033/ESGF/CMIP6.9755

Li, L. (2019). CAS FGOALS-g3 model output prepared for CMIP6 CMIP historical (Version 20221115) [Dataset]. *Earth System Grid Federation*. https://doi.org/10.22033/ESGF/CMIP6.3356

Liu, W., Fedorov, A. V., Xie, S.-P., & Hu, S. (2020). Climate impacts of a weakened Atlantic meridional overturning circulation in a warming climate. *Science Advances*, *6*(26), eaaz4876. https://doi.org/10.1126/sciadv.aaz4876

Liu, W., & Liu, Z. (2013). A diagnostic indicator of the stability of the Atlantic meridional overturning circulation in CCSM3. *Journal of Climate*, *26*(6), 1926–1938. https://doi.org/10.1175/JCLI-D-11-00681.1

Liu, W., & Liu, Z. (2014). A note on the stability indicator of the Atlantic meridional overturning circulation. *Journal of Climate*, *27*(2), 969–975. https://doi.org/10.1175/JCLI-D-13-00181.1

Liu, W., Liu, Z., & Brady, E. C. (2014). Why is the AMOC monostable in coupled general circulation models? *Journal of Climate*, *27*(6), 2427–2443. https://doi.org/10.1175/JCLI-D-13-00264.1

Liu, W., Liu, Z., & Hu, A. (2013). The stability of an evolving Atlantic meridional overturning circulation. *Geophysical Research Letters*, *40*(8), 1562–1568. https://doi.org/10.1002/grl.50365

Liu, W., Xie, S. P., Liu, Z., & Zhu, J. (2017). Overlooked possibility of a collapsed Atlantic meridional overturning circulation in warming climate. *Science Advances*, *3*(1), 1–8. https://doi.org/10.1126/sciadv.1601666

Locarnini, M. M., Mishonov, A. V., Baranova, O. K., Boyer, T. P., Zweng, M. M., Garcia, H. E., et al. (2018). In A. Mishonov Technical Editor (Ed.), *World Ocean Atlas 2018, volume 1: Temperature* Ref. NOAA Atlas NESDIS (Vol. 81, p. 52). Retrieved from https://archimer.ifremer.fr/doc/00651/76338/

Lovato, T., & Peano, D. (2020). CMCC CMCC-CM2-SR5 model output prepared for CMIP6 CMIP historical (Version 20221106) [Dataset]. *Earth System Grid Federation*. https://doi.org/10.22033/ESGF/CMIP6.3825

Lovato, T., Peano, D., & Butenschön, M. (2021). CMCC CMCC-ESM2 model output prepared for CMIP6 CMIP (Version 20221116) [Dataset]. *Earth System Grid Federation*. https://doi.org/10.22033/ESGF/CMIP6.13164

Majumder, S., Schmid, C., & Halliwell, G. (2016). An observations and model-based analysis of meridional transports in the South Atlantic. *Journal of Geophysical Research: Oceans*, *121*(8), 5622–5638. https://doi.org/10.1002/2016jc011693

Manabe, S., & Stouffer, R. J. (1988). Two stable equilibria of a coupled ocean-atmosphere model. *Journal of Climate*, *1*(9), 841–866. https://doi.org/10.1175/1520-0442(1988)001<0841:TSEOAC>2.0.CO;2

Manta, G., Speich, S., Karstensen, J., Hummels, R., Kersalé, M., Laxenaire, R., et al. (2021). The South Atlantic meridional overturning circulation and mesoscale eddies in the first GO-SHIP section at 34.5°S. *Journal of Geophysical Research: Oceans*, *126*(2), 1–25. https://doi.org/10.1029/2020JC016962

Masumoto, Y., Sasaki, H., Kagimoto, T., Komori, N., Ishida, A., Sasai, Y., et al. (2004). A fifty-year eddy-resolving simulation of the World Ocean: Preliminary outcomes of OFES (OGCM for the Earth simulator). *Journal of the Earth Simulator*, *1*, 35–36. https://doi.org/10.1109/oceans.2004.1406350

Matos, F. D. A. O., Pereira, J., & Dengler, M. (2020). Salinity biases and the variability of the Atlantic meridional overturning circulation in GFDL-CM3. *Ocean Science Journal*, *55*(4), 505–520. https://doi.org/10.1007/s12601-020-0040-8

McDonagh, E. L., & King, B. A. (2005). Oceanic fluxes in the South Atlantic. *Journal of Physical Oceanography*, *35*(1), 109–122. https://doi.org/10.1175/JPO-2666.1

McDonagh, E. L., King, B. A., Bryden, H. L., Courtois, P., Szuts, Z., Baringer, M., et al. (2015). Continuous estimate of Atlantic oceanic freshwater flux at 26.5°N. *Journal of Climate*, *28*(22), 8888–8906. https://doi.org/10.1175/JCLI-D-14-00519.1

Mecking, J. V., Drijfhout, S. S., Jackson, L. C., & Andrews, M. B. (2017). The effect of model bias on Atlantic freshwater transport and implications for AMOC bi-stability. *Tellus, Series A: Dynamic Meteorology and Oceanography*, *69*(1), 1–15. https://doi.org/10.1080/16000870.2017.1299910

Mecking, J. V., Drijfhout, S. S., Jackson, L. C., & Graham, T. (2016). Stable AMOC off state in an eddy-permitting coupled climate model. *Climate Dynamics*, *47*(7–8), 2455–2470. https://doi.org/10.1007/s00382-016-2975-0

Meinen, C. S., Speich, S., Piola, A. R., Ansorge, I., Campos, E., Kersalé, M., et al. (2018). Meridional overturning circulation transport variability at 34.5°S during 2009–2017: Baroclinic and barotropic flows and the dueling influence of the boundaries. *Geophysical Research Letters*, *45*(9), 4180–4188. https://doi.org/10.1029/2018GL077408

(NASA/GISS), N. G. I. for S. S. (2018). NASA-GISS GISS-E2.1G model output prepared for CMIP6 CMIP historical (Version 20221109) [Dataset]. *Earth System Grid Federation*. https://doi.org/10.22033/ESGF/CMIP6.7127

(NASA/GISS), N. G. I. for S. S. (2019). NASA-GISS GISS-E2-1-G-CC model output prepared for CMIP6 CMIP historical (Version 20221114) [Dataset]. *Earth System Grid Federation*. https://doi.org/10.22033/ESGF/CMIP6.11762

Park, S., & Shin, J. (2019). SNU SAM0-UNICON model output prepared for CMIP6 CMIP historical (Version 20221115) [Dataset]. *Earth System Grid Federation*. https://doi.org/10.22033/ESGF/CMIP6.7789

Perez, R. C., Garzoli, S. L., Meinen, C. S., & Matano, R. P. (2011). Geostrophic velocity measurement techniques for the meridional overturning: Circulation and meridional heat transport in the South Atlantic. *Journal of Atmospheric and Oceanic Technology*, *28*(11), 1504–1521. https://doi.org/10.1175/JTECH-D-11-00058.1

Pita, I., Goes, M., Volkov, D. L., Dong, S., Goni, G., & Cirano, M. (2024). An ARGO and XBT observing system for the Atlantic meridional overturning circulation and meridional heat transport (AXMOC) at 22.5°S. *Journal of Geophysical Research: Oceans*, *129*(1). https://doi.org/10.1029/2023jc020010

Pujol, M. I., Faugère, Y., Taburet, G., Dupuy, S., Pelloquin, C., Ablain, M., & Picot, N. (2016). DUACS DT2014: The new multi-mission altimeter data set reprocessed over 20 years. *Ocean Science*, *12*(5), 1067–1090. https://doi.org/10.5194/os-12-1067-2016

Rahmstorf, S. (1996). On the freshwater forcing and transport of the Atlantic thermohaline circulation. *Climate Dynamics*, *12*(12), 799–811. https://doi.org/10.1007/s003820050144

Ridley, J., Menary, M., Kuhlbrodt, T., Andrews, M., & Andrews, T. (2019). MOHC HadGEM3-GC31-LL model output prepared for CMIP6 CMIP historical (Version 20221108) [Dataset]. *Earth System Grid Federation*. https://doi.org/10.22033/ESGF/CMIP6.6109

Rienecker, M. M., Suarez, M. J., Gelaro, R., Todling, R., Bacmeister, J., Liu, E., et al. (2011). MERRA: NASA's modern-era retrospective analysis for research and applications. *Journal of Climate*, *24*(14), 3624–3648. https://doi.org/10.1175/JCLI-D-11-00015.1

Roemmich, D., & Gilson, J. (2009). The 2004-2008 mean and annual cycle of temperature, salinity, and steric height in the global ocean from the Argo Program. *Progress in Oceanography*, *82*(2), 81–100. https://doi.org/10.1016/j.pocean.2009.03.004

Roemmich, D., & Owens, B. (2000). The Argo project: Global ocean observations for understanding and prediction of climate variability. *Oceanography*, *13*(2), 45–50. https://doi.org/10.5670/oceanog.2000.33

Sasaki, H., Nonaka, M., Masumoto, Y., Sasai, Y., Uehara, H., & Sakuma, H. (2008). An eddy-resolving hindcast simulation of the quasiglobal ocean from 1950 to 2003 on the Earth simulator. In *High resolution numerical modelling of the atmosphere and ocean* (pp. 157–185). Springer New York. https://doi.org/10.1007/978-0-387-49791-4_10

Saunders, P. M., & King, B. A. (1995). Oceanic fluxes on the WOCE A11 section. *Journal of Physical Oceanography*, *25*(9), 1942–1958. https://doi.org/10.1175/1520-0485(1995)025<1942:OFOTWA>2.0.CO;2

Seferian, R. (2018). CNRM-CERFACS CNRM-ESM2-1 model output prepared for CMIP6 CMIP historical (Version 20221106) [Dataset]. *Earth System Grid Federation*. https://doi.org/10.22033/ESGF/CMIP6.4068

Seland, Ø., Bentsen, M., Oliviè, D. J. L., Toniazzo, T., Gjermundsen, A., Graff, L. S., et al. (2019). NCC NorESM2-LM model output prepared for CMIP6 CMIP historical (Version 20221116) [Dataset]. *Earth System Grid Federation*. https://doi.org/10.22033/ESGF/CMIP6.8036

Sitz, L. E., Farneti, R., & Griffies, S. M. (2015). Simulated South Atlantic transports and their variability during 1958–2007. *Ocean Modelling*, *91*, 70–90. https://doi.org/10.1016/j.ocemod.2015.05.001

Skliris, N., Marsh, R., Mecking, J. V., & Zika, J. D. (2020). Changing water cycle and freshwater transports in the Atlantic Ocean in observations and CMIP5 models. *Climate Dynamics*, *54*(11–12), 4971–4989. https://doi.org/10.1007/s00382-020-05261-y

Stommel, H. (1961). Thermohaline convection with two stable regimes of flow. *Tellus*, *13*(2), 224–230. https://doi.org/10.1111/j.2153-3490.1961.tb00079.x

Stouffer, R. (2019). UA MCM-UA-1-0 model output prepared for CMIP6 CMIP historical (Version 20221116) [Dataset]. *Earth System Grid Federation*. https://doi.org/10.22033/ESGF/CMIP6.8888

Sun, C., Thresher, A., Keeley, R., Hall, N., Hamilton, M., Chinn, P., et al. (2010). The data management system for the global temperature and salinity profile programme. In J. Hall, D. E. Harrison, & D. Strammer (Eds.), *Proceedings of OceanObs'09: Sustained Ocean Observations and Information for Society* (pp. 931–938). European Space Agency. https://doi.org/10.5270/OceanObs09.cwp.86

Swart, N. C., Cole, J. N. S., Kharin, V. V., Lazare, M., Scinocca, J. F., Gillett, N. P., et al. (2019). CCCma CanESM5 model output prepared for CMIP6 CMIP historical (Version 20221106) [Dataset]. *Earth System Grid Federation*. https://doi.org/10.22033/ESGF/CMIP6.3610

Talley, L. D. (2003). Shallow, intermediate, and deep overturning components of the global heat budget. *Journal of Physical Oceanography*, *33*(3), 530–560. https://doi.org/10.1175/1520-0485(2003)033<0530:SIADOC>2.0.CO;2

Tang, Y., Rumbold, S., Ellis, R., Kelley, D., Mulcahy, J., Sellar, A., et al. (2019). MOHC UKESM1.0-LL model output prepared for CMIP6 CMIP historical (Version 20221110) [Dataset]. *Earth System Grid Federation*. https://doi.org/10.22033/ESGF/CMIP6.6113

Tatebe, H., & Watanabe, M. (2018). MIROC MIROC6 model output prepared for CMIP6 CMIP historical (Version 20221107) [Dataset]. *Earth System Grid Federation*. https://doi.org/10.22033/ESGF/CMIP6.5603

Tsujino, H., Urakawa, L. S., Griffies, S. M., Danabasoglu, G., Adcroft, A. J., Amaral, A. E., et al. (2020). Evaluation of global ocean–sea-ice model simulations based on the experimental protocols of the Ocean Model Intercomparison Project phase 2 (OMIP-2). *Geoscientific Model Development*, *13*(8), 3643–3708. https://doi.org/10.5194/gmd-13-3643-2020

van Westen, R. M., Kliphuis, M., & Dijkstra, H. A. (2024). Physics-based early warning signal shows that AMOC is on tipping course. *Science Advances*, *10*(6). https://doi.org/10.1126/sciadv.adk1189

Vellinga, M., & Wood, R. A. (2002). Global climatic impacts of a collapse of the Atlantic thermohaline circulation. *Climatic Change*, *54*(3), 251–267. https://doi.org/10.1023/a:1016168827653

Voldoire, A. (2018). CMIP6 simulations of the CNRM-CERFACS based on CNRM-CM6-1 model for CMIP experiment historical (Version 20221106) [Dataset]. *Earth System Grid Federation*. https://doi.org/10.22033/ESGF/CMIP6.4066

Weber, S. L., & Drijfhout, S. S. (2007). Stability of the Atlantic meridional overturning circulation in the last glacial maximum climate. *Geophysical Research Letters*, *34*(22), 1–5. https://doi.org/10.1029/2007GL031437

Weijer, W., Cheng, W., Drijfhout, S. S., Fedorov, A. V., Hu, A., Jackson, L. C., et al. (2019). Stability of the Atlantic meridional overturning circulation: A review and synthesis. *Journal of Geophysical Research: Oceans*, *124*(8), 5336–5375. https://doi.org/10.1029/2019JC015083

Weijer, W., Cheng, W., Garuba, O. A., Hu, A., & Nadiga, B. T. (2020). CMIP6 models predict significant 21st century decline of the Atlantic meridional overturning circulation. *Geophysical Research Letters*, *47*(12). https://doi.org/10.1029/2019GL086075

Weijer, W., De Ruijter, W. P. M., Dijkstra, H. A., & Van Leeuwen, P. J. (1999). Impact of interbasin exchange on the Atlantic overturning circulation. *Journal of Physical Oceanography*, *29*(9), 2266–2284. https://doi.org/10.1175/1520-0485(1999)029<2266:IOIEOT>2.0.CO;2

Weijer, W., & Dijkstra, H. A. (2003). Multiple oscillatory modes of the global ocean circulation. *Journal of Physical Oceanography*, *33*(11), 2197–2213. https://doi.org/10.1175/1520-0485(2003)033<2197:MOMOTG>2.0.CO;2

Wu, T., Chu, M., Dong, M., Fang, Y., Jie, W., Li, J., et al. (2018). BCC BCC-CSM2MR model output prepared for CMIP6 CMIP historical (Version 20221109) [Dataset]. *Earth System Grid Federation*. https://doi.org/10.22033/ESGF/CMIP6.2948

Yan, X., Zhang, R., & Knutson, T. R. (2017). The role of Atlantic overturning circulation in the recent decline of Atlantic major hurricane frequency. *Nature Communications*, *8*(1), 1695. https://doi.org/10.1038/s41467-017-01377-8

Yin, J., & Stouffer, R. J. (2007). Comparison of the stability of the Atlantic thermohaline circulation in two coupled atmosphere–Ocean General circulation models. *Journal of Climate*, *20*(17), 4293–4315. https://doi.org/10.1175/JCLI4256.1

Zhang, J., Wu, T., Shi, X., Zhang, F., Li, J., Chu, M., et al. (2018). BCC BCC-ESM1 model output prepared for CMIP6 CMIP historical (Version 20221116) [Dataset]. *Earth System Grid Federation*. https://doi.org/10.22033/ESGF/CMIP6.2949

Ziehn, T., Chamberlain, M., Lenton, A., Law, R., Bodman, R., Dix, M., et al. (2019). CSIRO ACCESS-ESM1.5 model output prepared for CMIP6 CMIP historical (Version 20221106) [Dataset]. *Earth System Grid Federation*. https://doi.org/10.22033/ESGF/CMIP6.4272

Zweng, M. M., Reagan, J. R., Seidov, D., Boyer, T. P., Locarnini, M. M., Garcia, H. E., et al. (2019). In A. Mishonov Technical Editor (Ed.), *World Ocean Atlas 2018, volume 2: Salinity* Ref. NOAA Atlas NESDIS (Vol. 82, p. 50). Retrieved from https://archimer.ifremer.fr/doc/00651/76339/